scientific reports

Check for updates

OPEN

In vitro and in silico pharmacological effects of *Rosmarinus officinalis* leaf methanolic extracts and essential oils

Khalid Abdullah Alaboudi[1], Ibrahim M. Aziz[2]✉, Abdulaziz Abdullah Almosa[3], Mohamed A. Farrag[2], Tarad Abalkhail[2], Rawan M. Alshalan[2] & Abdulaziz M. Almuqrin[4]

Rosmarinus officinalis **L. has been widely used as a spice to enhance the shelf-life of food for centuries. While existing research in the literature suggests that the primary antibacterial component of this plant is its essential oil (EO), there is a lack of comparative studies employing both in vitro and in silico approaches to evaluate the antimicrobial, antioxidant, anticancer, and antidiabetic properties of *R. officinalis* leaf EO (ROLEO) and *R. officinalis* leaf methanolic extract (ROLME). The present study investigates the bioactive components and biological activities of ROLEO and ROLME using gas chromatography-mass spectrometry analysis. Additionally, the total phenolic content (TPC) and total flavonoid content (TFC) were quantified, and their antioxidant, antidiabetic, anticancer, and antibacterial activities were evaluated in vitro and in silico studies. GC–MS analysis revealed 20 bioactive compounds of ROLME, compared to 73 bioactive compounds in ROLEO. The TPC of ROLEO was higher, measuring 49.34 ± 2.84 mg GAE per gram of dry weight of the extract, compared to ROLME, which had a TPC of 38.13 ± 3.31 mg GAE per gram of dry weight of the extract. The TFC of ROLEO was measured at 24 ± 1.47 mg QE/g of dry weight, which is higher than that of ROLME, measured at 19 ± 1.47 mg QE/g of dry weight. Additionally, ROLEO demonstrated superior antioxidant activity at low concentrations compared to ROLME and greater antidiabetic properties by suppressing the actions of α-amylase and α-glucosidase enzymes. Moreover, ROLEO showed promising anticancer effects at lower doses, and antibacterial capabilities, particularly against Gram-positive bacteria. Molecular docking studies have identified key components of ROLEO that exhibit significant bioactivity. Among these compounds, 1H-Cycloprop[e]azulen-4-ol, decahydro-1,1,4,7-tetramethyl-, [1ar-(1α,4β,4aβ,7α,7aβ,7bα)]-demonstrated the highest activity against α-amylase, while thymol exhibited the strongest activity against caspase-3 and *E. coli* gyrase B. Overall, molecular docking and pharmacokinetic analysis identified promising inhibitory effects of key ROLEO compounds on α-amylase, caspase-3, and *E. coli* gyrase B, with favorable drug-like properties. These findings suggest that the EO of *R. officinalis* may serve as the basis for the development of innovative synthetic medications, offering valuable insights for the pharmaceutical industry to design novel treatments for various diseases.**

Keywords Antibacterial, Anticancer, Antidiabetic, Antioxidant, Essential oil, Molecular docking, *Salvia rosmarinus* Spenn.

Since ancient times, natural medicine has been used to cure a variety of illnesses. Initially, medicinal plants were utilized instinctively, taking inspiration from the behaviour of animals, as there was little knowledge

[1]Advanced Agricultural and Food Technologies Institute, King Abdulaziz City for Science and Technology (KACST), 11451 Riyadh, Saudi Arabia. [2]Department of Botany and Microbiology, College of Science, King Saud University, 11451 Riyadh, Saudi Arabia. [3]Wellness Prevention Medicine, King Abdulaziz City for Science and Technology (KACST), 11451 Riyadh, Saudi Arabia. [4]Department of Clinical Laboratory Sciences, College of Applied Medical Sciences, King Saud University, 12372 Riyadh, Saudi Arabia. ✉email: iaziz@ksu.edu.sa

about the causes of illnesses, the characteristics of plants, and their therapeutic applications. Natural remedies are becoming increasingly important because of the many benefits provided by their bioactive components. Furthermore, for many years, conventional plant-based medicines have been proven crucial for the treatment of a wide range of illnesses[1].

Lamiaceae (Mint family) is the sixth-largest *angiosperm* family and includes a diverse group of fragrant and medicinal plants. *Lamiaceae* and *Labiatae* are flowering plant families. Species of the genus *Salvia* constitute the largest genus of *Lamiaceae* family. *Rosmarinus officinalis* L. (*Salvia rosmarinus* Spenn., an isonym of *Salvia rosmarinus* Schleid is an aromatic evergreen shrub belonging to the *Lamiaceae* family. In a recent evolutionary analysis, the genera *Salvia* and *Rosmarinus* were combined to become *Salvia Rosmarinus*[2].

R. officinalis (Rosemary) grows naturally in dry scrubs and rocky terrain in the Mediterranean regions of southern Europe and western Asia. Owing to its medicinal qualities, rosemary is used in traditional medicine as an oral preparation to treat dysmenorrhea, muscular spasms, and renal colic[3]. In Saudi Arabia's desert villages, *R. officinalis* grows wild and is frequently used in traditional medicine[4]. *R. officinalis* leaves have been acknowledged as a basic material. The leaf extracts of *R. officinalis* contain flavonoids such as luteolin, nepetin, nepitrin, and apigenin), as well as phenolic acids (e.g., caffeic acid, betulinic acid, ursolic acid, carnosic acid and caffeic acid)[5].

The biological activities *of R. officinalis's* secondary metabolites and extracts have been documented in studies examining a range of effects, including heart remodeling following myocardial infarction, body weight fluctuations, dyslipidemia, cerebral ischemia, hepato-nephrotoxicity, stress, anxiety, as well as antioxidant, antitumor, anti-infectious, anti-inflammatory, and analgesic properties[6]. Prior phytochemical studies of *R. officinalis* have focused on the antifungal properties of its essential oil (EO)[2]. In a recent study, the methanolic extract of *S. rosmarinus* leaves exhibited significant growth inhibition at a concentration of 300 µg/mL against three fungal isolates obtained from symptomatic strawberry plants, *Botrytis cinerea* (OR116486), *Fusarium oxysporum* (OR116505), and *Rhizoctonia solani* (OR116525)[6]. In addition to antifungal effects, *R. officinalis* extracts exhibit strong antioxidant properties, attributed mainly to rosmarinic acid, a polyphenol identified in the leaf extractas it was documented from *R. officinalis* leaf extracts isolated from Northern Riyadh, Saudi Arabia[7]. Recent studies have also revealed the antiproliferative and cytotoxic effects of *R. officinalis* EO against Jurkat, MCF-7, HT-29, and HeLa[7]. Antidiabetic effects of *R. officinalis* have also been reported, demonstrating its therapeutic potential in managing diabetes-related complications[8].

Molecular docking is a frequently used computational approach for predicting the interactions between bioactive compounds and their potential target proteins. This method is particularly valuable for evaluating plant extracts by identifying compounds interacting with specific molecular targets associated with various disease[9]. Molecular docking plays a crucial role in facilitating virtual screening, empowering researchers to systematically rank compounds for further experimental validation while simultaneously enhancing their understanding of the underlying mechanisms of these molecules[10]. Molecular docking can identify compounds in *R. officinalis* leaf essential oil (ROLEO) and *R. officinalis* leaf methanolic extracts (ROLME) that bind strongly to key therapeutic targets, including enzymes involved in cancer proliferation (e.g., caspase-3), bacterial survival (e.g., DNA gyrase B), and diabetes (e.g., α-amylase)[11]. By analyzing binding scores, hydrogen bonding, and hydrophobic interactions, researchers can estimate the potential pharmacological effects associated with specific chemicals in the extracts[12,13].

Pharmacokinetics refers to the examination of how a substance is absorbed, distributed, metabolized, excreted, and its potential toxicity (ADMET) within the organism[14]. The ADMET profiles of individual chemicals within plant extracts may be estimated using in silico methods that assess various parameters, including oral bioavailability, the capacity to penetrate the blood–brain barrier, and metabolic stability[15]. Essential parameters including molecular weight, lipophilicity (logP), the presence of hydrogen bond donors and acceptors, as well as polar surface area, are employed to evaluate whether these compounds adhere to Lipinski's rule of five, a guideline that forecasts drug-likeness[16]. The combination of molecular docking and pharmacokinetic predictions offers comprehensive insights into the potential of plant-derived pharmaceuticals, guiding subsequent in vitro and in vivo investigations[17].

Although earlier research has extensively investigated the cytotoxic and antibacterial properties of ROLEO, a comparison of its antimicrobial, antioxidant, and anticancer properties with those of ROLME has not been carried out. In this study, we used gas chromatography-mass spectrometry (GC–MS) analysis to determine which bioactive elements were most prevalent in ROLEO and ROLME. Using 1,1-diphenyl-2-picryl hydrazyl (DPPH) scavenging and 2,2′-azino-bis (3-ethylbenzothiazoline-6-sulfonic acid) (ABTS) assays, we assessed the phytochemical composition and antioxidant properties of ROLEO in comparison to ROLME. In addition, we aimed to evaluate the possible effects of ROLEO in comparison to ROLME against MCF-7 breast cancer cells and hepatocellular carcinoma (HepG2) cells, as well as to clarify the underlying mechanism using reverse transcription polymerase chain reaction (RT-PCR)-based mRNA expression profiles of particular pro- and anti-apoptosis marker genes. Evaluation of the antidiabetic activity of ROLEO and ROLME will focus on α-amylase and α-glucosidase. ROLEO and ROLME's antibacterial effectiveness against gram-positive and gram-negative bacteria was examined using the minimum inhibitory concentration (MIC) and minimum bactericidal concentration (MBC) methods. This research yields novel insights into the pharmacological potential of *R. officinalis*, particularly its ability to induce apoptosis in cancer cell lines and its robust antibacterial, antioxidant, and antidiabetic properties.

Results

Extraction yields

The extraction yield, calculated based on dry matter weight (w/w), demonstrated that the ROLME extraction process achieved a yield of 30.87 ± 3.24%Meanwhile, the ROLEO extraction process a lower yield of 3.74 ± 0.75% (v/w).

Chemical composition of ROLEO and ROLME

GC–MS was used to examine the bioactive elements, ROLEO and ROLME. Seventy-three peaks were recorded for the bioactive components of ROLEO, which were identified by comparing their peak retention time (RT), peak area (%), molecular formula (MF), and molecular weight (MW) with those of known compounds listed in the NIST library. Phenol, 2-methyl-5-(1-methylethyl), was the main component of ROLEO, accounting for 42.52% of the total. *p*-Cymene (6.48%), bicyclo [3.1.0] hexan-3-one, 4-methyl-1-(1-methylethyl)-, [1S-(1α,4β,5α)] (5.72%), and (+)-2-Bornanone (4.94%) (Table 1 and Fig. 1). However, the findings showed that tetrahydropyranylethylene glycol, accounting for 21.33% of the total, was the primary compound in ROLME. The compounds that followed were Bergamotol, Z-α-trans-(14.91%), and Benzofran-3-one, 2-[3,4-dihydroxybenzylidene]-6-hydroxy-(21.02%) (Table 2 and Fig. 2).

Total phenolic content (TPC) and total flavonoid content (TFC) of ROLEO and ROLME

The findings revealed that the ROLEO had a higher total phenolic content (TPC) of 49.34 ± 2.84 mg GAE/g of dry extract ($R^2 = 0.994$) compared to ROLME, which had a TPC of 38.13 ± 3.31 mg GAE/g of dry extract ($R^2 = 0.911$). Additionally, the total flavonoid content (TFC) for ROLEO was 24 ± 1.47 mg QE/g of dry extract ($R^2 = 0.935$), while ROLME had a TFC of 19 ± 1.47 mg QE/g of dry extract ($R^2 = 0.899$).

DPPH and ABTS radical scavenging activity

DPPH and ABTS radical scavenging assays were used to compare the antioxidant activities of ROLEO and ROLME, with ascorbic acid as the positive control (Fig. 3). At high ROLEO and ROLME concentrations, both DPPH and ABTS assays demonstrated greater antioxidant activity. However, compared to the positive control (IC_{50} value: 28.11 ± 1.14 µg/mL), ROLEO and ROLME were less effective ($P < 0.05$). The DPPH scavenger effect of ROLEO (IC_{50} value: 93.41 ± 17.15 µg/mL) was found to be much higher ($P < 0.05$) than that of ROLME with an IC_{50} value of 172.42 ± 1.24 µg/mL). Similarly, ROLEO (IC_{50} value: 90.71 ± 2.15 µg/mL) exhibited significant ($P < 0.05$) antioxidant activity against the ABTS free radical than ROLME (IC_{50} value: 163.11 ± 2.12 µg/mL).

Cell cytotoxicity

The anticancer efficacy of ROLEO and ROLME against MCF-7 and HepG2 cells was examined using an MTT assay. MTT assay revealed that ROLEO and ROLME reduced the viability of MCF-10A, MCF-7, and HepG2 cells in a dose-dependent manner. Remarkably, ROLEO and ROLME showed good anticancer activity against MCF-7 and HepG2 cells compared with the positive control (cisplatin 30 µg/mL). ROLEO appeared to be more effective with IC_{50} values of 156.12 ± 0.94 µg/mL and 125.82 ± 2.14 µg/mL, respectively than ROLME in both tested MCF-7 and HepG2 cells, with IC_{50} values of 348.12 ± 1.34 µg/mL and 241.95 ± 1.14 µg/mL, respectively, these results were milder than standard drug IC_{50} values, which were 29.32 ± 2.15 and 22.42 ± 1.34 µg/mL, respectively. Nevertheless, neither ROLEO nor ROLME significantly impacted the normal human epithelial breast cell line MCF-10A (Fig. 4A,B).

Apoptotic analysis

Figure 5 shows the effect of ROLEO and ROLME on the activity of anti-apoptotic genes (Bcl-xL and Bcl-2) and apoptotic genes (*caspase-3*, *8*, *9*, and *Bax*). MCF-7 and HepG2 cells treated with ROLEO and ROLME exhibited significant upregulation of apoptotic gene activity compared to untreated control and anti-apoptotic genes ($P < 0.05$). *Caspases-3*, *-8*, *-9*, and *Bax* were found to be more highly expressed in MCF-7 and HepG2 cells than in ROLEO cells. MCF-7 and HepG2 cells treated with ROLEO and ROLME had a lower expression of anti-apoptotic genes (*Bcl-xL* and *Bcl-2*) than the untreated control group ($P < 0.05$). In contrast, ROLEO and ROLME had no significant impact on the expression of anti-apoptotic genes (Bcl-*xL* and *Bcl-2*) or apoptotic genes (*caspases-3*, *-8*, *-9*, and *Bax*) in MCF-10A cells compared to the untreated control cells (Fig. 5A and B).

Morphological changes in cells

To visualize and assess the morphological changes induced by ROLEO and ROLME in MCF-7, HepG2, and MCF-10A cell lines, cells were treated with 100 µg/mL of either ROLEO and ROLME and incubated for 48 h under a controlled condition (37 °C, 5% CO_2, 95% air) in a humidified incubator. The changes were then visualized using an inverted microscope (Eclipse TS100, Nikon, Japan). Compared to untreated-MCF-7 and HepG2 cells (negative control) (Fig. 6A,E) and MCF-10A cells treated with the positive control (ribavirin) (Fig. 6B,F), MCF-7 and HepG2 cells treated with ROLEO exhibited more pronounced morphological changes, including cell rounding, the formation of small aggregates, and progressive detachment (Fig. 6C,G), compared to those treated with ROLME (Fig. 6D,H). In contrast, the morphology of MCF-10A cells treated with ROLEO (Fig. 6K) or ROLME (Fig. 6L) resembled that of the untreated MCF-10A cells (negative control) and those treated with ribavirin (positive control) (Fig. 6I,J). This observation suggests that ROLEO has a strong inhibitory effect.

In vitro α-amylase and α-glucosidase inhibition activities

In vitro α-amylase and α-glucosidase inhibitory assays were used to assess the antidiabetic potential of ROLEO and ROLME, and their IC_{50} values were determined. In comparison to acarbose, ROLEO showed a considerable inhibitory action against α-amylase and α-glucosidase ($IC_{50} = 174 \pm 2.14$ µg/mL and 156.62 ± 1.23 µg/mL, respectively) (Fig. 7A), whereas ROLME inhibited α-amylase ($IC_{50} = 243 \pm 0.24$ µg/mL), α-glucosidase ($IC_{50} = 216.62 \pm 0.22$ µg/mL) (Fig. 7B). The standard drug, acarbose showed inhibitory efficacy against α-amylase ($IC_{50} = 24.45 \pm 0.108$ µg/mL) and α-glucosidase ($IC_{50} = 18.52 \pm 1.98$ µg/mL).

Peak	Rt	Area	Area%	Name	MF	MW(g/mol)
1	4.857	5,475,188	0.03	2,5-Cyclooctadien-1-ol	C_8H1_2O	124
2	5.643	104,545,936	0.65	α-Pinene	$C_{10}H_{16}$	136
3	5.781	126,438,927	0.79	(1R)-2,6,6-Trimethylbicyclo[3.1.1]hept-2-ene	$C_{10}H_{16}$	136
4	6.095	180,391,734	1.12	Camphene	$C_{10}H_{16}$	136
5	6.821	62,000,369	0.38	Bicyclo[3.1.1]heptane, 6,6-dimethyl-2-methylene-, (1S)-	$C_{10}H_{16}$	136
6	6.948	119,531,374	0.74	1-Octen-3-ol	$C_8H_{16}O$	128
7	7.105	31,833,373	0.19	3-Octanone	$C_8H_{16}O$	128
8	7.202	109,175,969	0.68	β-Myrcene	$C_{10}H_{16}$	136
9	7.859	64,992,609	0.407	1,3-Cyclohexadiene, 1-methyl-4-(1-methylethyl)-	$C_{10}H_{16}$	136
10	8.124	1,036,039,670	6.48	*p*-Cymene	$C_{10}H_{14}$	134
11	8.189	134,025,408	0.83	1,3,8-p-Menthatriene	$C_{10}H_{14}$	134
12	8.294	650,447,686	4.07	Eucalyptol	$C_{10}H_{18}O$	154
13	9.007	143,877,921	0.91	γ-Terpinene	$C_{10}H_{16}$	136
14	9.257	112,502,646	0.71	Bicyclo[3.1.0]hexan-2-ol, 2-methyl-5-(1-methylethyl)-, (1α,2α,5α)-	$C_{10}H_{18}O$	154
15	9.844	14,841,559	0.09	Cyclohexene, 1-methyl-4-(1-methylethylidene)-	$C_{10}H_{16}$	136
16	9.988	18,180,554	0.11	cis-1,2-Cyclohexanediol	$C_6H_{12}O_2$	116
17	10.121	20,224,405	0.12	Bicyclo[3.1.0]hexan-2-ol, 2-methyl-5-(1-methylethyl)-, (1α,2α,5α)-	$C_{10}H_{18}O$	154
18	10.191	49,545,065	0.31	Linalool	$C_{10}H_{18}O$	154
19	10.319	274,009,082	1.71	Thujone	$C_{10}H_{16}O$	152
20	10.686	913,664,125	5.72	Bicyclo[3.1.0]hexan-3-one, 4-methyl-1-(1-methylethyl)-, [1S-(1α,4β,5α)]-	$C_{10}H_{16}O$	152
21	11.424	789,391,639	4.94	(+)-2-Bornanone	$C_{10}H_{16}O$	152
22	12.009	152,388,167	0.95	Bicyclo[2.2.1]heptan-2-ol, 1,7,7-trimethyl-, (1S-endo)-	$C_{10}H_{18}O$	154
23	12.19	29,851,271	0.18	Terpinen-4-ol	$C_{10}H_{18}O$	154
24	12.328	141,005,393	0.88	α-Terpineol	$C_{10}H_{18}O$	154
25	12.704	43,310,975	0.27	L-α-Terpineol	$C_{10}H_{18}O$	154
26	13.092	52,623,358	0.32	Terpineol	$C_{10}H_{18}O$	154
27	13.439	26,535,110	0.16	1,2,2,3-Tetramethylcyclopent-3-enol	$C_9H_{16}O$	140
28	14.221	739,395,470	4.63	Benzene, 2-methoxy-1-methyl-4-(1-methylethyl)-	$C_{11}H_{16}O$	164
29	14.895	17,194,801	0.11	Cyclohexanone, 5-methyl-2-(1-methylethylidene)-	$C_{10}H_{16}O$	152
30	15.316	12,855,409	0.08	Acetic acid, 1,7,7-trimethyl-bicyclo[2.2.1]hept-2-yl ester	$C_{12}H_{20}O_2$	196
31	15.388	18,192,277	0.11	Caryophyllene	$C_{15}H_{24}$	204
32	15.564	186,650,401	1.16	Thymol	$C_{10}H_{14}O$	150
33	16.27	6,791,413,362	42.52	Phenol, 2-methyl-5-(1-methylethyl)-	$C_{10}H_{14}O$	150
34	16.336	16,626,499	0.11	Ascaridole epoxide	$C_{10}H_{16}O_3$	184
35	17.555	11,022,789	0.06	3-Hydroxy-2-(2-methylcyclohex-1-enyl)propionaldehyde	$C_{10}H_{16}O_2$	168
36	17.686	21,147,845	0.13	Bergamotol, Z-α-trans	$C_{15}H_{24}O$	220
37	17.757	20,204,198	0.12	α-Copaene	$C_{15}H_{24}$	204
38	17.998	16,349,104	0.10	(-)-β-Bourbonene	$C_{15}H_{24}$	204
39	18.932	732,292,706	4.58	Caryophyllene	$C_{15}H_{24}$	204
40	19.104	19,150,531	0.11	1H-Cyclopropa[a]naphthalene, 1a,2,3,5,6,7,7a,7b-octahydro-1,1,7,7a-tetramethyl-, [1aR-(1aα,7α,7aα,7bα)]-	$C_{15}H_{24}$	204
41	19.261	10,552,245	0.06	(-)-α-Panasinsen	$C_{15}H_{24}$	204
42	19.376	127,172,652	0.79	Aromandendrene	$C_{15}H_{24}$	204
43	19.475	11,995,235	0.07	(1S,4aR,7R)-1,4a-Dimethyl-7-(prop-1-en-2-yl)-1,2,3,4,4a,5,6,7-octahydronaphthalene	$C_{15}H_{24}$	204
44	19.623	60,528,051	0.37	1H-Benzocycloheptene, 2,4a,5,6,7,8,9,9a-octahydro-3,5,5-trimethyl-9-methylene-,	$C_{15}H_{24}$	204
45	19.753	266,730,729	1.67	Humulene	$C_{15}H_{24}$	204
46	19.915	55,740,132	0.34	Alloaromadendrene	$C_{15}H_{24}$	204
47	20.221	11,000,944	0.06	Azulene, 1,2,3,3a,4,5,6,7-octahydro-1,4-dimethyl-7-(1-methylethenyl)-, [1R-(1α,3aβ,4α	$C_{15}H_{24}$	204
48	20.301	64,643,364	0.40	γ-Muurolene	$C_{15}H_{24}$	204
49	20.6	24,354,585	0.15	Longifolene-(V4)	$C_{15}H_{24}$	204
50	20.764	124,113,583	0.77	1H-Cycloprop[e]azulene, 1a,2,3,5,6,7,7a,7b-octahydro-1,1,4,7-tetramethyl-, [1aR-(1aα,7α,7aβ,7bα)]-	$C_{15}H_{24}$	204
51	20.901	122,136,678	0.76	1H-Benzocycloheptene, 2,4a,5,6,7,8-hexahydro-3,5,5,9-tetramethyl-, (R)-	$C_{15}H_{24}$	204
52	21.07	50,861,734	0.31	β-Bisabolene	$C_{15}H_{24}$	204
53	21.22	82,507,095	0.51	Naphthalene, 1,2,3,4,4a,5,6,8a-octahydro-7-methyl-4-methylene-1-(1-methylethyl)-, (1α,4aβ,8aα)-	$C_{15}H_{24}$	204
54	21.442	158,472,824	0.99	Naphthalene, 1,2,3,5,6,8a-hexahydro-4,7-dimethyl-1-(1-methylethyl)-, (1S-cis)-	$C_{15}H_{24}$	204
55	21.568	9,718,882	0.06	γ-Dehydro-ar-himachalene	$C_{15}H_{20}$	200
56	21.776	12,260,089	0.07	β-Guaiene	$C_{15}H_{24}$	204

Continued

Peak	Rt	Area	Area%	Name	MF	MW(g/mol)
57	21.905	7,692,138	0.04	α-Calacorene	$C_{15}H_{24}$	204
58	22.758	127,700,894	0.79	1H-Cycloprop[e]azulen-7-ol, decahydro-1,1,7-trimethyl-4-methylene-, [1ar-(1aα,4aα,7β,7aβ,7bα)]-	$C_{15}H_{24}O$	220
59	22.883	125,630,878	0.78	Caryophyllene oxide	$C_{15}H_{24}O$	220
60	23.104	220,279,383	1.37	1H-Cycloprop[e]azulen-4-ol, decahydro-1,1,4,7-tetramethyl-, [1aR-(1aα,4β,4aβ,7α,7aβ,7bα)]-	$C_{15}H_{26}O$	222
61	23.244	13,053,257	0.08	trans-Z-α-Bisabolene epoxide	$C_{15}H_{24}O$	220
62	23.485	53,882,098	0.33	(1R,3E,7E,11R)-1,5,5,8-Tetramethyl-12-oxabicyclo[9.1.0]dodeca-3,7-diene	$C_{15}H_{24}O$	220
63	24.003	19,517,579	0.12	Calarene epoxide	$C_{15}H_{24}O$	220
64	24.097	23,628,116	0.14	10,10-Dimethyl-2,6-dimethylenebicyclo[7.2.0]undecan-5β-ol	$C_{15}H_{24}O$	220
65	24.19	30,260,506	0.18	.tau.-Cadinol	$C_{15}H_{26}O$	222
66	24.497	12,254,330	0.07	α-Cadinol	$C_{15}H_{26}O$	222
67	24.567	23,076,465	0.14	Isoaromadendrene epoxide	$C_{15}H_{24}O$	220
68	24.861	26,884,648	0.16	(1R,7S,E)-7-Isopropyl-4,10-dimethylenecyclodec-5-enol	$C_{15}H_{24}O$	220
69	25.132	14,929,495	0.09	α-Bisabolol	$C_{15}H_{26}O$	222
70	29.699	11,704,103	0.07	1,3-Dioxolan-2-one, 5-methyl-4-(4,4-dimethyl-2,3-dimethylenecyclohexyl)	$C_{14}H_{20}O_3$	236
71	30.255	20,550,489	0.12	9-Hexadecenoic acid	$C_{16}H_{30}O_2$	254.41
72	32.693	25,092,303	0.15	1-Naphthalenepropanol, α-ethenyldecahydro-α,5,5,8a-tetramethyl-2-methylene-, [1S-[1α(R*),4aβ,8aα	$C_{20}H_{34}O$	290
73	34.154	10,564,009	0.06	2-[4-methyl-6-(2,6,6-trimethylcyclohex-1-enyl)hexa-1,3,5-trienyl]cyclohex-1-en-1-carboxaldehyde	$C_{23}H_{32}O$	324

Table 1. GC–MS compounds in ROLEO.

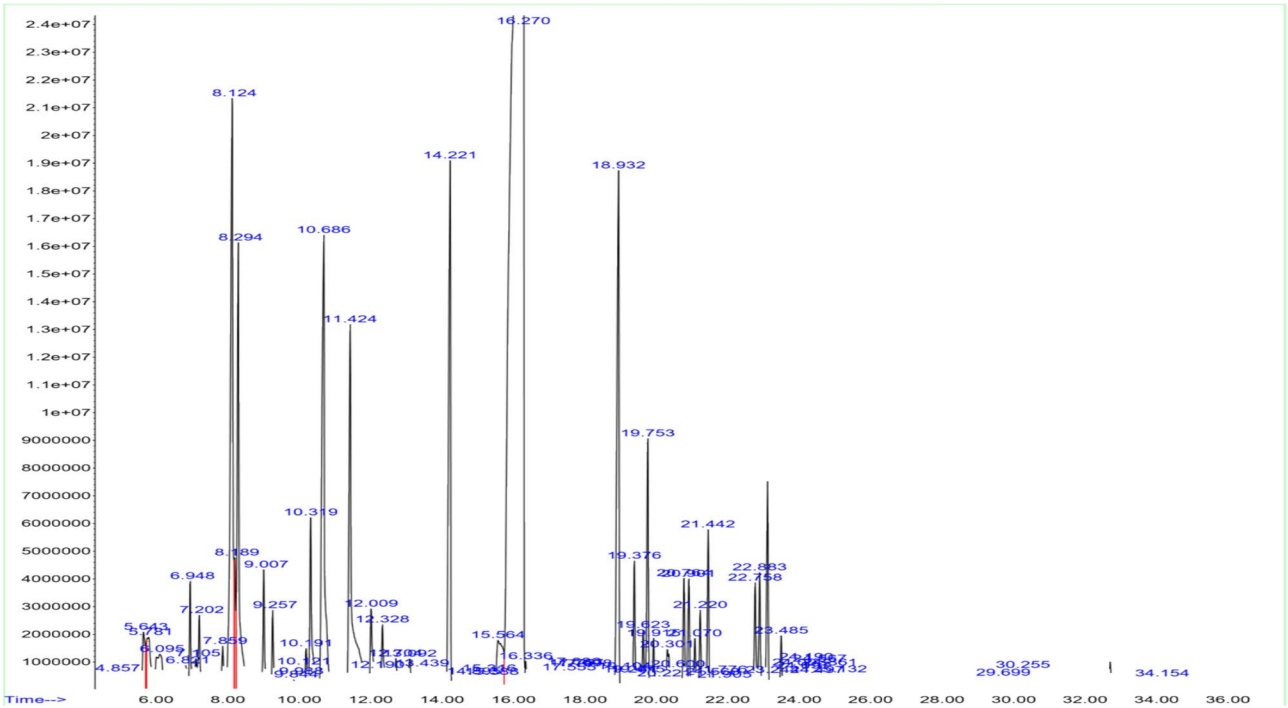

Fig. 1. The GC–MS chromatograms of ROLEO. All spectral peaks correlate with identified chemicals, with a big peak indicating the primary constituent of the extract.

Antibacterial effects of ROLEO and ROLME

The antibacterial activity was evaluated by using the disc diffusion technique, which showed that ROLEO and ROLME inhibited the bacterial growth of all tested bacteria in a dose-dependent manner compared to the controls. The results shown in Tables 3 and 4 indicate that the ROLEO (MIC values = 4.68 ± 2.21—25 ± 0.00 µg/mL) had more antibacterial activity in comparison to the ROLME (MIC values = 12.50 ± 0.00—25 ± 0.00 µg/mL). Importantly, Gram-positive bacteria were more susceptible to ROLEO than Gram-negative bacteria (Tables 3 and 4).

Peak	Rt (min)	Area	Area%	Name	MF	MW(g/mol)
1	9.51	11,763,886	2.79	4H-Pyran-4-one, 2,3-dihydro-3,5-dihydroxy-6-methyl-	$C_6H_8O_4$	144.12
2	10.354	2,140,388	0.51	Spiro[2.2]pentane-1-carboxylic acid	$C_6H_8O_2$	112.13
3	10.7	2,899,922	0.68	β-Guaiene	$C_{15}H_{24}$	204
4	11.214	1,751,855	0.41	l-Gala-l-ido-octose	$C_8H_{16}O_8$	240.21
5	11.858	12,941,043	3.07	n-Propyl 9,12-octadecadienoate	$C_{21}H_{38}O_2$	322.287
6	12.77	2,937,233	0.69	Diazoprogesterone	$C_{21}H_{28}N_2O_2$	338.247
7	13.215	9,755,046	2.31	Bisabolol oxide B	$C_{15}H_{26}O_2$	238.37
8	13.381	6,307,979	1.49	(S)-2,2,6-Trimethyl-6-((S)-4-methylcyclohex-3-en-1-yl)dihydro-2H-pyran-3(4H)-one	C15H24O2	236.35
9	13.663	26,312,297	6.24	Verbenone	$C_{10}H_{14}O$	150.22
10	13.776	89,911,781	21.33	Tetrahydropyranylethyleneglycol	$C_7H_{14}O_3$	146.18
11	14.381	3,841,938	0.91	9-Hexadecenoic acid	$C_{16}H_{30}O_2$	254.41
12	14.466	62,793,664	14.91	Bergamotol, Z-α-trans	$C_{15}H_{24}O$	220.183
13	14.514	11,891,044	2.82	1,6-Dioxaspiro [4.4]non-3-ene, 2-(2,4-hexadiynylidene)-	$C_{13}H_{12}O_2$	200.23
14	14.6	2,809,351	0.67	Cyclopropanebutanoic acid, 2-[[2-[[2-[(2-pentylcyclopropyl) methyl]cyclopropyl]methyl]cyclopropyl]methyl]-, methyl ester	$C_{25}H_{42}O_2$	374.6
15	14.776	23,657,663	5.61	n-Hexadecanoic acid	$C_{16}H_{32}O_2$	256.42
16	15.196	2,789,548	0.66	Benz[e]azulene-3,8-dione, 5-[(acetyloxy)methyl]-3a,4,6a,7,9,10,10a,10b-octahydro-3a,10a-dihydroxy-2,10-dimethyl-,	$C_{19}H_{24}O_6$	348.4
17	15.309	5,750,927	1.36	Ethanol, 2-(9-octadecenyloxy)-, (Z)-	$C_{20}H_{40}O_2$	312.5
18	15.513	3,446,669	0.817	10-Octadecenoic acid, methyl ester	$C_{19}H_{36}O_2$	296.5
19	15.694	15,190,939	3.61	9,12-Octadecadienoic acid (Z,Z)-	$C_{18}H_{32}O_2$	280.4
20	15.728	20,838,640	4.94	9,12,15-Octadecatrienoic acid, (Z,Z,Z)-	$C_{18}H_{30}O_2$	278.4
21	22.356	13,079,178	3.10	2-Cyclohexyl-2,5-cyclohexadiene-1,4-dione, 4-oxime	$C_{12}H_{15}NO_2$	205.25
22	22.984	88,591,972	21.02	Benzofran-3-one, 2-[3,4-dihydroxybenzylidene]-6-hydroxy-	$C_{15}H_{10}O_5$	270.24

Table 2. GC–MS compounds in ROLME.

Molecular docking analysis of ROLEO and ROLME

The inhibition of α-amylase is a key therapeutic strategy in controlling postprandial blood glucose surges in diabetic patients. Molecular docking results revealed that the antidiabetic activity of ROLEO against α-amylase was driven by three potent inhibitore: 1H-Cycloprop[e]azulen-4-ol, decahydro-1,1,4,7-tetramethyl-, [1ar-(1aalpha,4beta,4abeta,7alpha,7abeta,7balpha)]-, Thymol, and Phenol, 2-methyl-5-(1-methylethyl)- with glide scores of − 5.043, − 4.754, and − 4.692 kcal/mol respectively. While the activity of ROMEO showed its strongest antidiabetic activity through Benzofran-3-one, 2-[3,4-dihydroxybenzylidene]-6-hydroxy-, Bisabolol oxide B, and Verbenone with a glide gscore of − 6.149, − 4.957, and − 4.762 kcal/mol respectively (Table 5).

The activation of caspase-3 plays a crucial role in anticancer activity as it disrupts the apoptotic pathways that cancer cells often exploit to evade programmed cell death. Caspase-3 is a key executioner enzyme in apoptosis, responsible for cleaving specific cellular substrates, leading to cell dismantling and death.

The molecular docking analysis of anticancer compounds in ROLEO identified two potent caspase-3 inhibitors: Thymol, Bicyclo[3.1.0]hexan-3-one, 4-methyl-1-(1-methylethyl), and Phenol, 2-methyl-5-(1-methylethyl), with glide scores of − 5.458, − 5.190, and − 4.680 kcal/mol. While the anticancer activity of ROMEO against caspase-3 revealed that that 4H-Pyran-4-one, 2,3-dihydro-3,5-dihydroxy-6-methyl-, Benzofran-3-one, 2-[3,4-dihydroxybenzylidene]-6-hydroxy-, and Verbenone were the most active molecules with a glide gscore of − 5.989, − 5.847, and − 5.606 kcal/mol (Table 5).

The antibacterial activity of ROLEO was analyzed against *E. coli* gyrase B demonstrated strong inhibitory effects, with Thymol, Benzene, 2-methoxy-1-methyl-4-(1-methylethyl)-, and Phenol, 2-methyl-5-(1-methylethyl)- with a glide gscore of − 5.783, − 5.725, and − 5.573 kcal/mol. While in the inhibition of ROMEO to *E. coli* gyrase B was through Benzofran-3-one, 2-[3,4-dihydroxybenzylidene]-6-hydroxy-, 1,6-Dioxaspiro [4.4]non-3-ene, 2-(2,4-hexadiynylidene)-, (S)-2,2,6-Trimethyl-6-((S)-4-methylcyclohex-3-en-1-yl)dihydro-2H-pyran-3(4H)-one with a glide gscore of − 7.231, − 6.174, and − 5.766 kcal/mol (Table 5).

The 2D and 3D interaction between the compounds identified in ROLEO and the different active sites showed that 1H-Cycloprop[e]azulen-4-ol, decahydro-1,1,4,7-tetramethyl-, [1ar-(1aalpha,4beta,4abeta,7alpha,7abeta,7balpha)]- established a single hydrogen bond with the ASP 300 residue in the active site of α-amylase (Figs. 8A and 9A). In addition, thymol established a single hydrogen bond with the SER B 205 residue in the active site of caspase-3 (Figs. 8B and 9B). This molecule established a single Pi-cation type bond in the active site of *E. coli* gyrase B (Figs. 8C and 9C).

Furthermore, the 2D and 3D interaction analysis between the compounds identified in ROLME and the different active sites revealed that Benzofran-3-one, 2-[3,4-dihydroxybenzylidene]-6-hydroxy- established three hydrogen bonds with residues ASP197, ASP 300, and GLN 63 and two Pi-Pi stacking bonds with residue TRP 59 (Figs. 8D and 9D). This molecule formed one hydrogen bond with residue ASP 73 and one Pi-cation bond with residue ARG 76 in the active site of *E. coli* gyrase B (Figs. 8F and 9F).

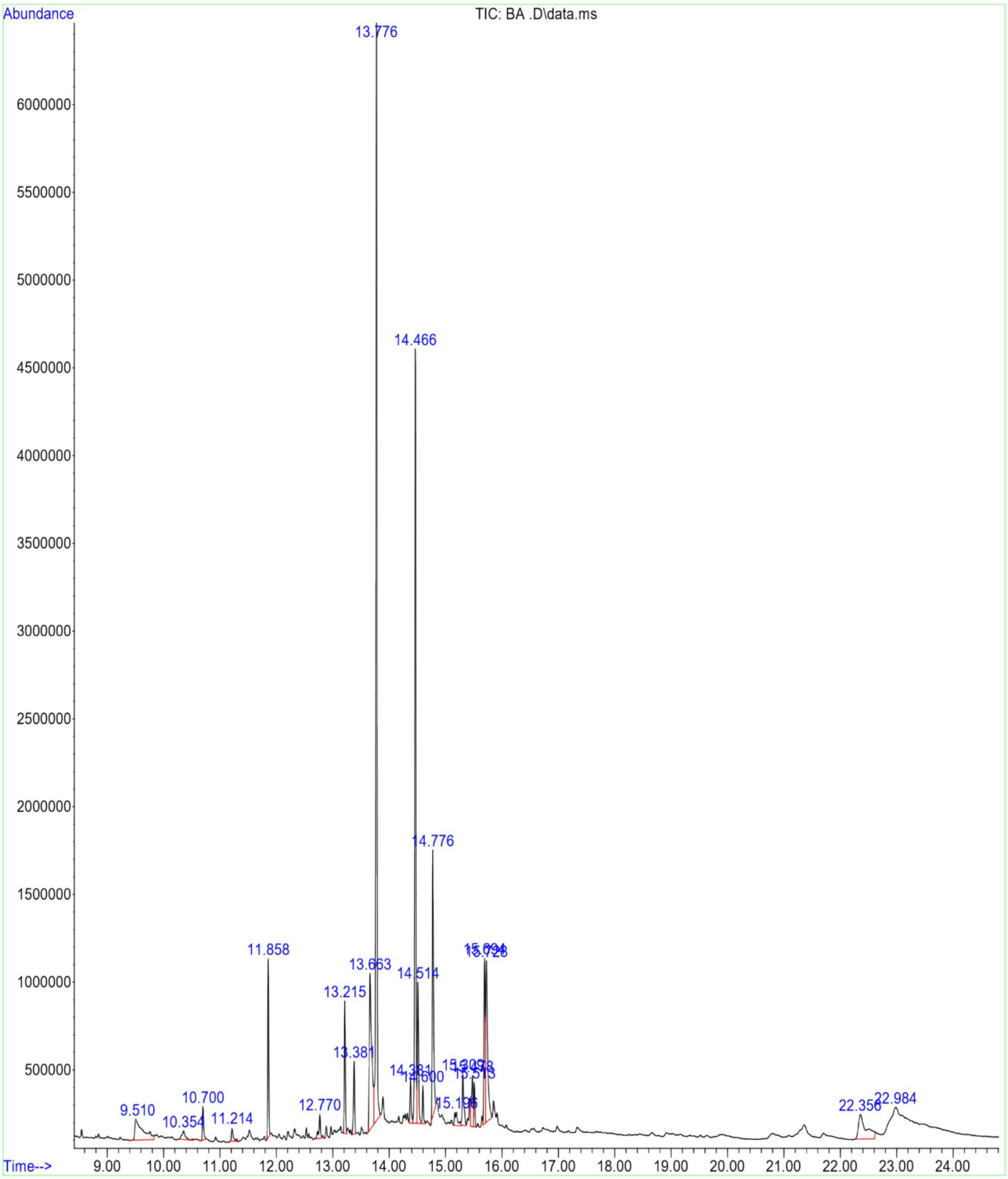

Fig. 2. The GC–MS chromatograms of ROLME. A prominent peak in the spectrum indicates the major component of the extract, and every peak that is seen corresponds to a recognized chemical.

In the active site of caspase-3, 4H-Pyran-4-one, 2,3-dihydro-3,5-dihydroxy-6-methyl- established two hydrogen bonds with residues HIS A: 121 and CYS A: 163 and one salt bridge with residue ARG A: 64 (Figs. 8E and 9E).

Prediction of ADMET by computational analysis

All ROLEO and ROMEO molecules presented acceptable physicochemical and pharmacokinetic values. Thymol and 1H-Cycloprop[e]azulen-4-ol, decahydro-1,1,4,7-tetramethyl-, [1ar-(1α,4β,4aβ,7α,7aβ,7bα)]- which is

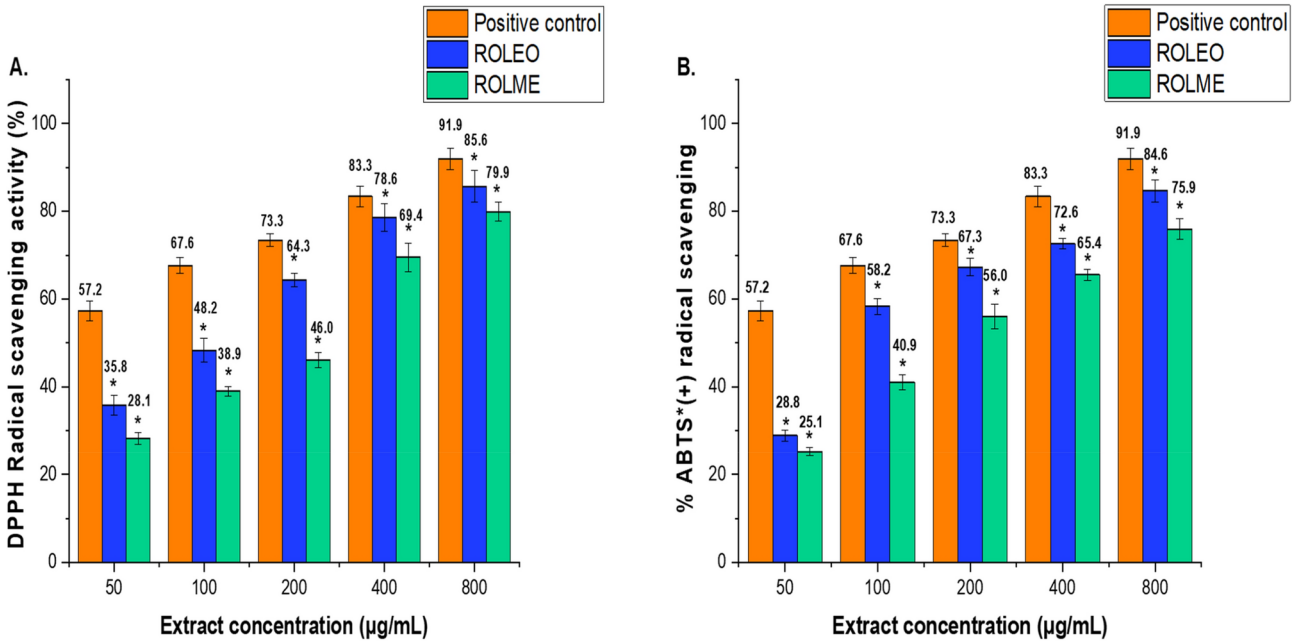

Fig. 3. Antioxidant activity of ROLEO and ROLME (**A**), DPPH reducing power and (**B**), ABTS•(+) scavenging activity) at various concentrations (50–400 µg/mL). An ascorbic acid (250 µg/mL) was used as a positive control. The results are the mean ± SD of three different experiments. The scavenging activity of ROLEO and ROLME was significantly lower (*) than the positive control at a significance level of $P < 0.05$. • + = radical cation.

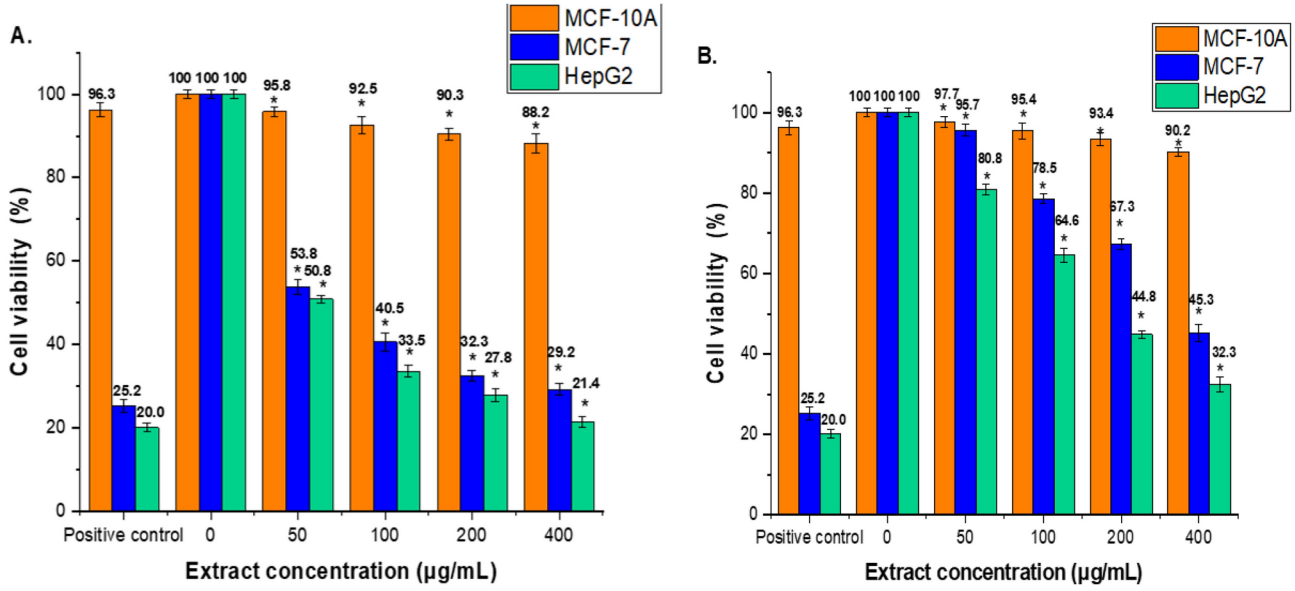

Fig. 4. The effect of ROLEO (**A**) and ROLME (**B**) on the viability of MCF-10A, MCF-7, and HepG2 cells using the MTT assay. Cells were treated with ROLEO and ROLME (0–400 µg/mL) for 24 h. Mean ± SD is presented from three independent experiments; the positive control was (cisplatin 30 µg/mL). (* = $P < 0.05$ compared to non-treated cells (negative control)).

among the most active ROLEO molecules against the proteins studied presented a molar mass of 150.22 and 222.37 g/mol and a total solvent accessible surface area of 391.249 and 458.88 radius, Predicted apparent Caco-2 cell permeability of 3835.969 and 5183.091 nm/s and a human oral percentage of 100% respectively (Table 6).

Benzofuran-3-one, 2-[3,4-dihydroxybenzylidene]-6-hydroxy- and 4H-Pyran-4-one, 2,3-dihydro-3,5-dihydroxy-6-methyl- which is among the most active ROMEO molecules against the proteins studied presented a molar mass of 270.241 and 144.127 g/mol and a Donor of hydrogen bonds < 5 and Acceptor of hydrogen

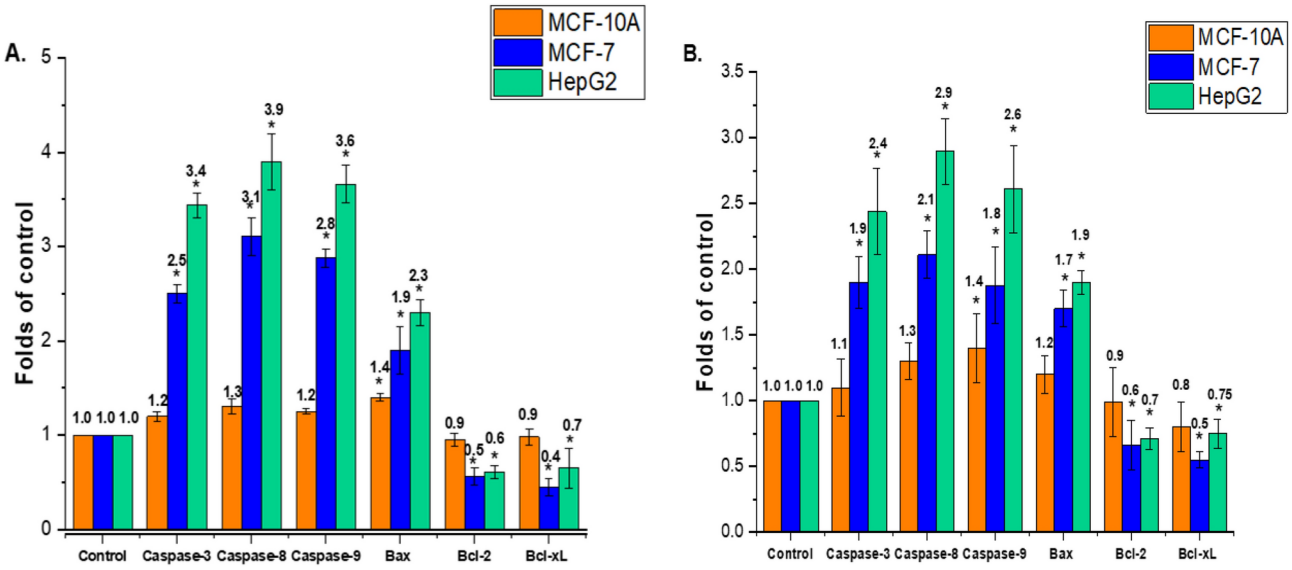

Fig. 5. Effect of ROLEO (**A**) and ROLME (**B**) on MCF-10A, MCF-7, and HepG2 cell lines and analysis of pro- and genes *caspase-3*, *-8* and *-9*, and *Bax*), and anti-apoptosis marker (*Bcl-2* and *Bcl-Xl*) genes. Cells were exposed to 100 µg/mL of ROLEO and ROLME for 48 h. Gene expression is represented as the mean ± SD of three independent experiments, (* = $P < 0.05$ compared to non-treated cells (control)).

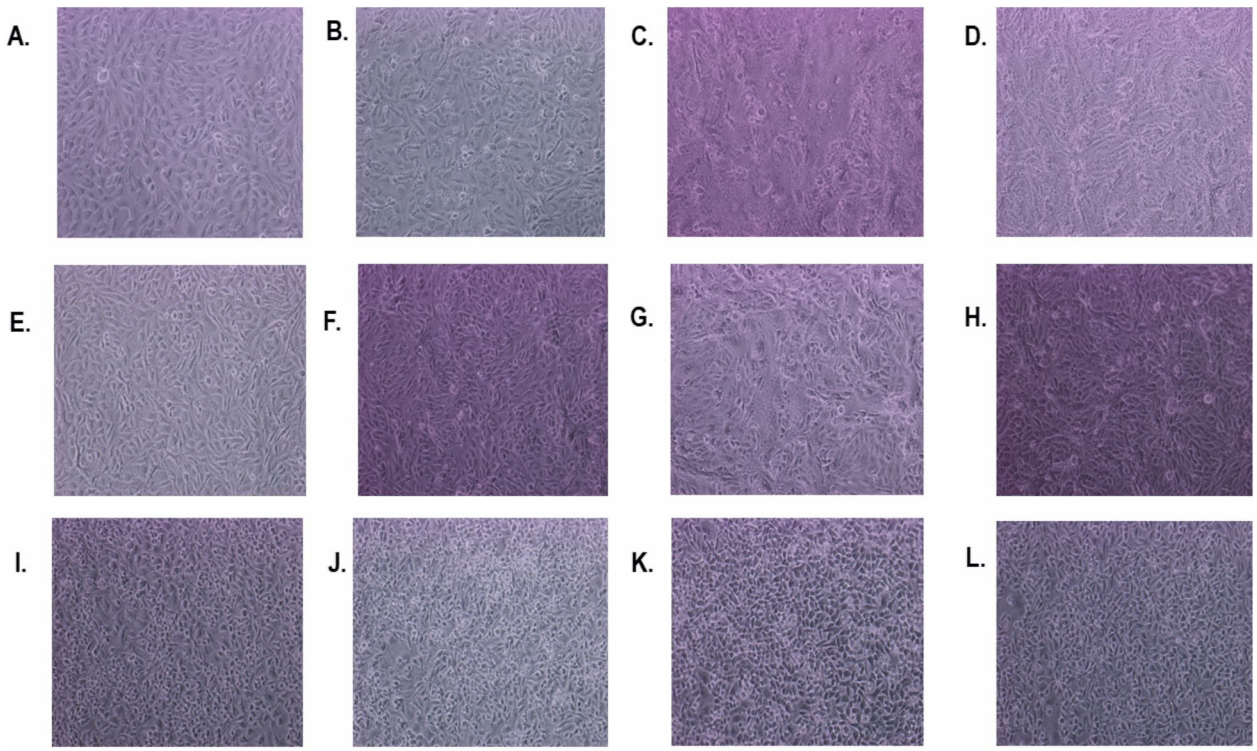

Fig. 6. The effect of ROLEO and ROLME on the MCF-7, HepG2, and MCF-10A cells morphology. Cells were exposed to 100 µg/mL of ROLEO and ROLME for 48 h. (**A**) represents MCF-7 non-treated cells, (**B**) represents MCF-7-treated cells with positive control (cisplatin 30 µg/mL), (**C**) represents MCF-7 -treated cells with ROLEO, (**D**) represents MCF-7 -treated cells with ROLME, (**E**) represents HepG2 non-treated cells, (**F**) = represents HepG2-treated cells with positive control (cisplatin 30 µg/mL), (**G**) represents HepG2-treated cells with ROLEO, (**H**) represents HepG2-treated cells with ROLME, (**I**) represents MCF-10A non-treated cells, (**J**) = represents MCF-10A -treated cells with positive control (cisplatin 30 µg/mL), (**K**) represents MCF-10A -treated cells with ROLEO , (**L**) represents MCF-10A -treated cells with ROLME. (Magnification power 10X).

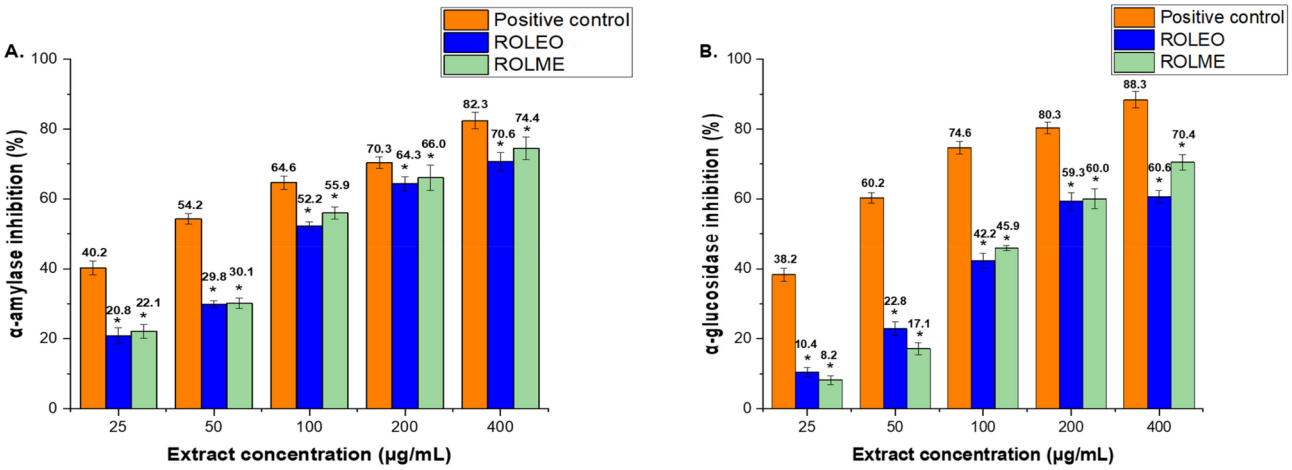

Fig. 7. Effect of ROLEO (**A**) and ROLME (**B**) on α-Amylase and α-glucosidase inhibitory activities at various concentrations (25–400 µg/mL). The results are the mean values of three replicates. The results are the mean ± SD of three experiments (* = $P < 0.05$ compared to the positive control).

Bacterium/dilution	Positive control	400 µg/mL	200 µg/mL	100 µg/mL	50 µg/mL	MIC (µg/mL)	MBC (µg/mL)
S. aureus	27 ± 0.61	25 ± 2.55	21 ± 2.21*	18 ± 1.48*	14 ± 2.34*	4.68 ± 2.21	6.25 ± 0.00
S. epidermidis	25 ± 1.57	22 ± 1.41*	16 ± 2.84*	14 ± 2.36*	11 ± 1.12*	6.25 ± 0.00	12.50 ± 0.00
E. faecalis	24 ± 2.42	22 ± 1.35*	18 ± 1.34*	15 ± 1.25*	11 ± 2.24*	6.25 ± 0.00	12.50 ± 0.00
E. coli	29 ± 1.12	20 ± 2.61*	17 ± 1.57*	15 ± 1.33*	8 ± 0.29*	25 ± 0.00	50 ± 0.00
K. pneumoniae	25 ± 1.33	23 ± 1.34*	20 ± 1.32*	16 ± 1.96*	10 ± 1.73*	12.50 ± 0.00	25 ± 0.00
P. aeruginosa	26 ± 2.68	19 ± 1.38*	16 ± 1.96*	13 ± 1.14*	9 ± 1.30*	12.50 ± 0.00	25 ± 0.00

Table 3. The inhibitory zone (mm), MIC (µg/mL), and MBC (µg/mL) of ROLEO. The reported values represent the mean of three separate experiments, with the standard deviation (SD) indicating the variability within the data. The asterisk (*) denotes statistical significance lower than positive control (Chloramphenicol, 25 µg/ml) with $P < 0.01$.

Bacterium/dilution	Positive control	400 µg/mL	200 µg/mL	100 µg/mL	50 µg/mL	MIC (µg/mL)	MBC (µg/mL)
S. aureus	27 ± 0.61	17 ± 2.71*	14 ± 0.34*	11 ± 2.35*	6 ± 1.65*	25 ± 0.00	50.00 ± 0.00
S. epidermidis	25 ± 1.57	19 ± 0.93*	14 ± 1.42*	11 ± 1.93*	7 ± 1.71*	12.50 ± 0.00	25.00 ± 0.00
E. faecalis	24 ± 2.42	18 ± 1.32*	16 ± 1.96*	13 ± 1.74*	8 ± 0.38*	25 ± 0.00	50.00 ± 0.00
E. coli	29 ± 1.12	22 ± 0.85*	17 ± 1.24*	13 ± 1.43*	11 ± 1.32*	12.50 ± 0.00	50.00 ± 0.00
K. pneumoniae	25 ± 1.33	20 ± 3.92*	17 ± 0.89*	13 ± 1.83*	9 ± 0.22*	25 ± 0.00	50.00 ± 0.00
P. aeruginosa	26 ± 2.68	19 ± 2.59*	16 ± 1.33*	12 ± 2.36*	10 ± 1.62*	12.50 ± 0.00	25.00 ± 0.00

Table 4. The inhibitory zone (mm), MIC (µg/mL), and MBC (µg/mL) of ROLME**.** The reported values are shown in triplicate as mean ± SD. The results demonstrate a statistically significant decrease from the positive control (25 µg/ml of chloramphenicol), indicated by (* = $P < 0.01$).

bonds ≤ 10, Predicted blood–brain partition coefficient of − 1.21 and − 0.603 and a human oral percentage of 73.036 and 78.38% respectively (Table 6).

Discussion

R. officinalis is widely distributed, yet only a limited number of studies have been conducted on this speciesThis study utilized in vitro and in silico techniques to investigate and characterize the bioactive components found in ROLEO and ROLME. Our in vitro assays, which include antibacterial, antidiabetic, antioxidant, and anticancer testing, aid in determining the safety and effectiveness of the discovered compounds. Additionally, molecular docking and other in silico techniques were employedto investigate possible interactions with significant biological targets, facilitating a deeper comprehension of the molecular mechanisms underlying their impacts. This integrated approach, combining chemical profiling alongside biological and computational analysis,

		Glide gscore (kcal/mol)		
		α-amylase (PDB :1B2Y)	Caspase-3 (PDB :3GJQ)	*E. coli* gyrase B (PDB: 3G7E)
ROLEO	(+)-2-Bornanone	− 4.376	− 4.167	− 5.038
	1H-Cycloprop[e]azulen-4-ol, decahydro-1,1,4,7-tetramethyl-, [1ar-(1aalpha,4beta,4abeta,7alpha,7abeta, 7balpha)]-	− 5.043	− 4.676	− 5.451
	Benzene, 2-methoxy-1-methyl-4-(1-methylethyl)-	− 3.929	− 4.593	− 5.725
	Bicyclo[3.1.0]hexan-3-one, 4-methyl-1-(1-methylethyl)-,	− 4.67	− 5.19	− 5.566
	Camphene	− 3.53	− 4.328	− 4.905
	Caryophyllene	− 3.526	− 3.717	− 4.368
	Eucalyptol	− 3.705	− 3.461	− 4.743
	Humulene	− 3.717	− 4.186	− 5.158
	p-Cymene	− 4.006	− 4.405	− 5.389
	Phenol, 2-methyl-5-(1-methylethyl)-	− 4.692	− 4.68	− 5.573
	Thujone	− 4.244	− 4.254	− 5.495
	Thymol	− 4.754	− 5.458	− 5.783
ROLME	(S)-2,2,6-Trimethyl-6-((S)-4-methylcyclohex-3-en-1-yl)dihydro-2H-pyran-3(4H)-one	− 4.374	− 4.368	− 5.766
	1,6-Dioxaspiro [4.4]non-3-ene, 2-(2,4-hexadiynylidene)-	− 4.109	− 5.121	− 6.174
	2-Cyclohexyl-2,5-cyclohexadiene-1,4-dione, 4-oxime	− 4.321	− 4.498	− 5.196
	4H-Pyran-4-one, 2,3-dihydro-3,5-dihydroxy-6-methyl-	− 4.693	− 5.898	− 4.96
	9,12,15-Octadecatrienoic acid, (Z,Z,Z)-	0.572	− 4.545	− 1.439
	9,12-Octadecadienoic acid (Z,Z)-	0.423	− 3.853	− 1.152
	Benzofran-3-one, 2-[3,4-dihydroxybenzylidene]-6-hydroxy-	− 6.002	− 5.7	− 7.084
	Bergamotol, Z-alpha-trans	− 4.179	− 4.381	− 4.828
	Bisabolol oxide B	− 4.957	− 5.028	− 5.582
	Ethanol, 2-(9-octadecenyloxy)-, (Z)-	− 3.197	− 2.506	− 4.277
	n-Hexadecanoic acid	1.578	− 3.455	− 0.26
	n-Propyl 9,12-octadecadienoate	− 2.553	− 2.536	− 5.008
	Tetrahydropyranylethyleneglycol	− 4.647	− 4.456	− 4.28
	Verbenone	− 4.762	− 5.606	− 5.569

Table 5. Docking results of ROLEO and ROMEO in different receptors.

facilitates the discovery of promising chemicals and the differentiation between useful and potentially harmful substances.

This study investigated both ROLEO and ROLME, with the findings showing that ROLME extraction yield 30.87 ± 3.24%, as determined by dry matter weight (w/w), while ROLEO achieved a lower yield of 3.74 ± 0.75% (v/w). The yield differences of ROLME and ROLEO is contingent upon several factors, including the portion of the plant used, the drying method applied, the solvent concentration, the extraction process length, and additional processing variables. Extraction yields are generally expressed as a percentage of the plant's dry weight, leading to a broad spectrum of bioactive substances, such as phenolic acids, flavonoids, and sesquiterpene lactones[18]. Several studies compared the use of different solvents in extracting different plant parts of *R. officinalis*. In this regard, a previous research effort demonstrated that the methanolic extraction of *R. officinalis* aerial parts achieved a yield of 30.87 ± 3.2%. In contrast, EO yields were found to be 1.14 ± 0.15 (v/w)[19]. In comparison to other studies, El Kamli et al. (2017) indicated that the yield values of EO from Moroccan rosemary ranged from 2.14% to 2.25% (v/w)[20]. Cutillas et al.[21] revealed that the yield of EO extracted from the aerial parts of *R. officinalis* from Spain ranged from 0.8 to 1.1%. (v/w).

GC–MS examination of ROLEO revealed that the primary components were the phenol, 2-methyl-5-(1-methylethyl), p-Cymene (6.48%), bicyclo [3.1.0], hexan-3-one, 4-methyl-1-(1-methylethyl)-, [1S-(1α,4β,5α)], and (+)-2-Bornanone. Whereas, 2-[3,4-dihydroxybenzylidene]-6-hydroxy, tetrahydropyranylethylene glycol, Bergamotol, Z-α-trans, and Benzofran-3-one were the main component of ROLME. Research conducted on the EO extracted from *R. officinalis* leaves identified 31 distinct compounds, which together represented 98.4% of the total oil content. The GC–MS analysis highlighted limonene (21.7%) and α-pinene (13.5%) as the primary hydrocarbons, while camphor (21.6%) and Z-linalool oxide (10.8%) were noted as the principal oxygenated monoterpenes[22]. A previous study using GC–MS analysis on the aerial parts of *R. officinalis* EO found 29 chemical components, and the main constituents were 1,8-cineole (43.77%), camphor (12.53%), and α-pinene (11.51%)[23]. A recent study on the spontaneous *R. officinalis* EO identified 31 compounds, which constitute 97.03% of the total composition, through GC–MS analysis, the primary constituents include camphor (41.22%) and 1,8-cineole (4.90%) classified as oxygenated monoterpenes, α-bisabolol (1.15%) categorized as a sesquiterpene, and amphene (18.14%) and α-pinene (17.49%) recognized as monoterpene hydrocarbons[19]. Tunisian rosemary is mainly composed of α-pinene (7.09–13.66%), camphene (3.09–5.07%), β-pinene (3.26–

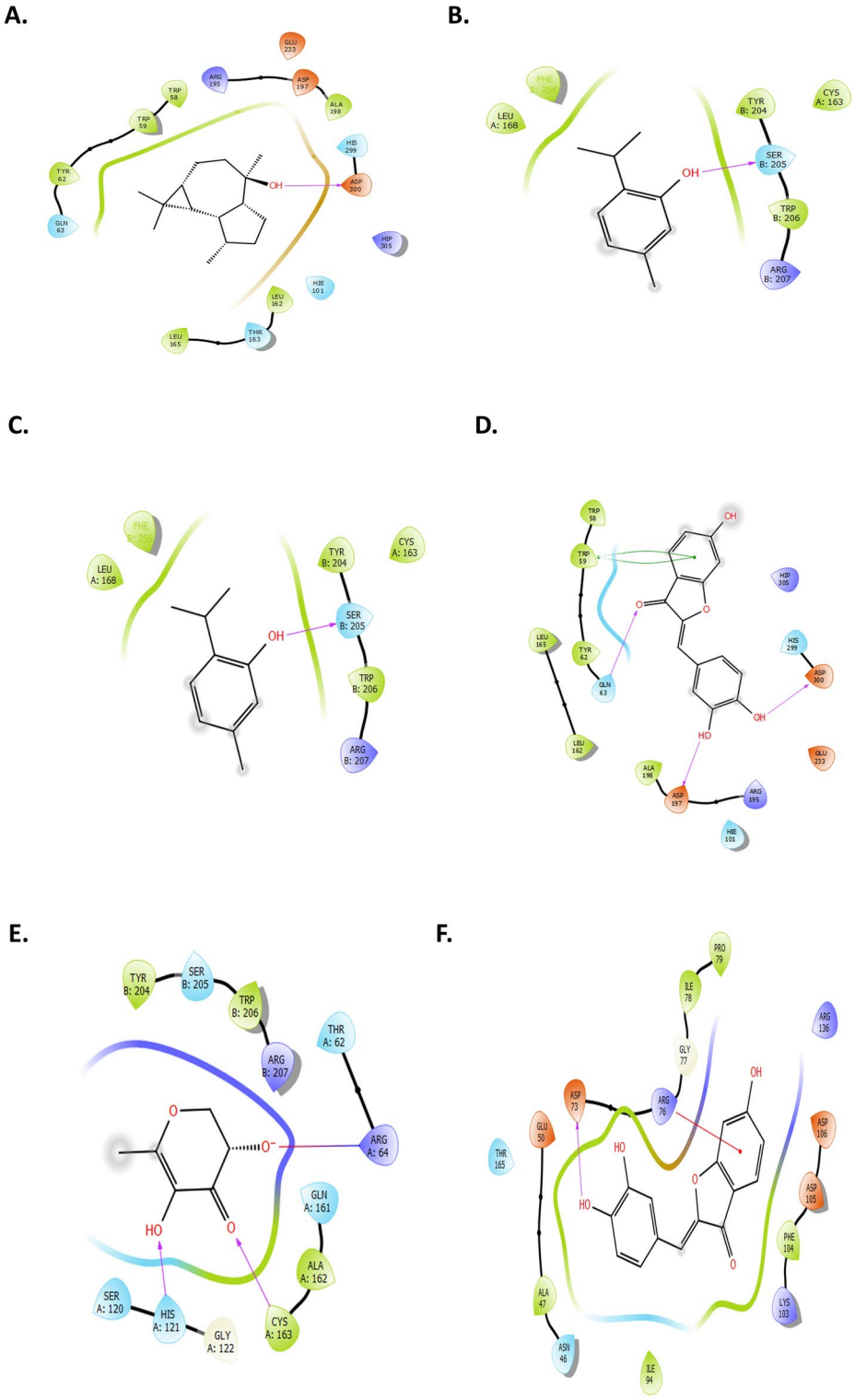

Fig. 8. The 2D viewer of ligands interactions with the active site. (**A**): 21H-Cycloprop[e]azulen-4-ol, decahydro-1,1,4,7-tetramethyl-, [1ar-(1aalpha,4beta,4abeta,7alpha,7abeta,7balpha)]- interactions with the active site of α-amylase. (**B** and **C**): Thymol interactions with caspase-3 and *E. coli* gyrase B active sites. (**D** and **F**): Benzofran-3-one, 2-[3,4-dihydroxybenzylidene]-6-hydroxy- interactions with the active sites of α-amylase and *E. coli* gyrase B. (**E**): 4H-Pyran-4-one, 2,3-dihydro-3,5-dihydroxy-6-methyl- interaction with the active site of caspase-3.

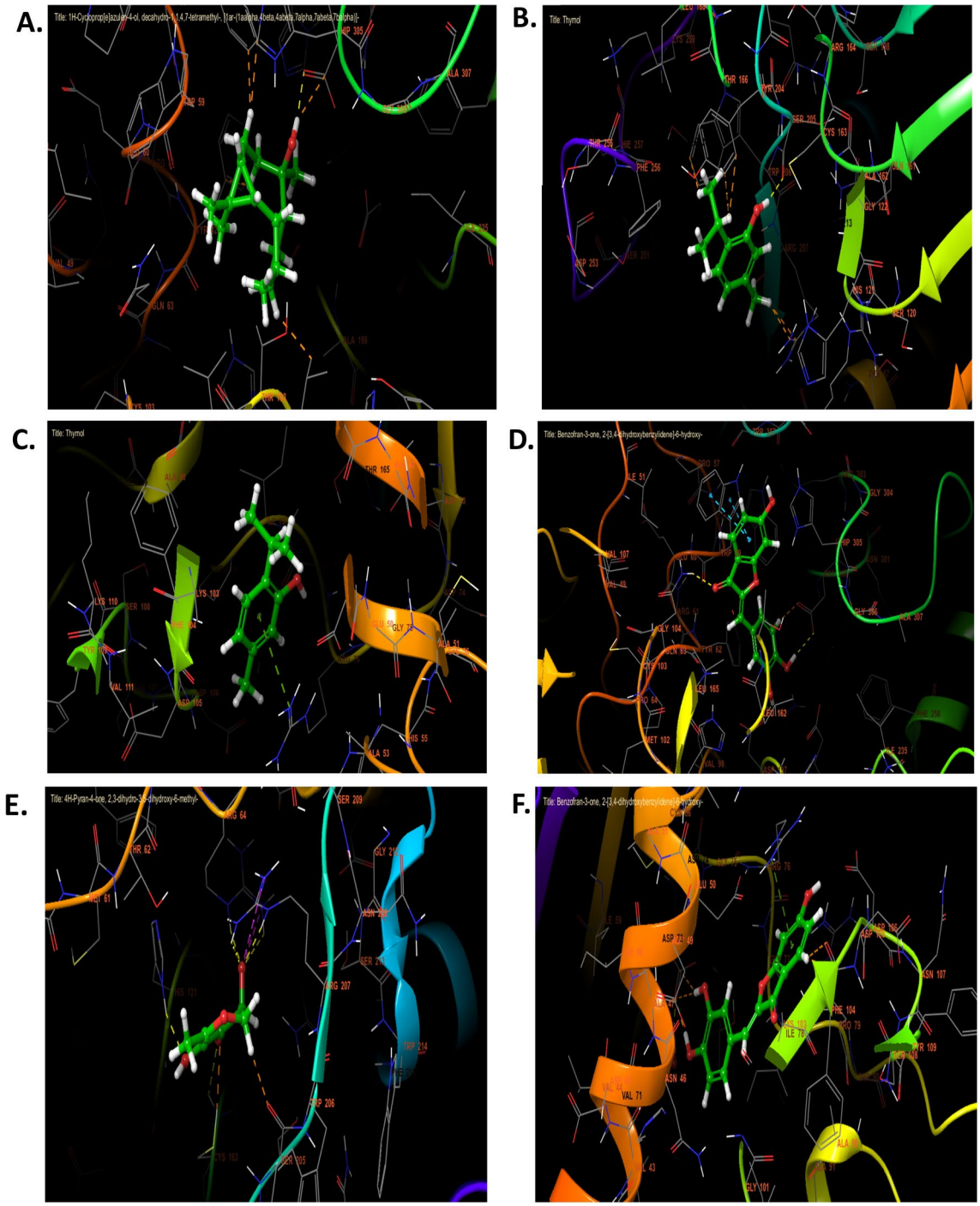

Fig. 9. The 3D viewer of ligands interactions with the active site. (**A**): 21H-Cycloprop[e]azulen-4-ol, decahydro-1,1,4,7-tetramethyl-, [1ar-(1aalpha,4beta,4abeta,7alpha,7abeta,7balpha)]-interactions with the active site of α-amylase. (**B** and **C**): Thymol interactions with caspase-3 and *E. coli* gyrase B active sites. (**D** and **F**): Benzofran-3-one, 2-[3,4-dihydroxybenzylidene]-6-hydroxy- interactions with the active sites of α-amylase and *E. coli* gyrase B. (**E**): 4H-Pyran-4-one, 2,3-dihydro-3,5-dihydroxy-6-methyl- interaction with the active site of caspase-3.

3.81%), cineole (46.8–57.88%), camphor (9.27–18.99%), and borneol (4.49–13.21%) using GC–MS analysis[24]. The biological effects of a number of these substances were previously studied. For example, carvacrol (2-methyl-5-(1-methyl ethyl) phenol) is a monoterpene phenol that is present in a variety of *Lamiaceae* species EOs[25]. Carvacrol has been demonstrated to have a wide range of biological effects, including antibacterial, antifungal, insecticidal, antioxidant, and anticancer properties[26]. *p*-cymene, also called *p*-cymol or *p*-isopropyltoluene, is an aromatic chemical with an alkyl substituent that is naturally found in the EOs of a variety of aromatic plants. The

		mol MW	SASA	donorHB	accptHB	QPlogPo/w	QPPCaco	QPlogBB	%HOA
ROLEO	p-CYMENE	134.221	383.117	0	0	3.648	9906.038	0.7	100
	Camphene	136.236	356.991	0	0	3.31	9906.038	0.855	100
	Eucalyptol	154.252	375.194	0	0.75	2.435	9906.038	0.6	100
	Bicyclo[3.1.0]hexan-3-one, 4-methyl-1 -(1-methylethyl)-, [1S-(1alpha,4beta,5alpha)]-	152.236	382.658	0	2	2.085	3504.948	0.134	100
	(+)-2-Bornanone	152.236	358.696	0	2	1.929	4128.173	0.27	100
	Benzene, 2-methoxy-1-methyl-4 -(1-methylethyl)-	164.247	411.576	0	0.75	3.19	9906.038	0.494	100
	Thymol	150.22	391.249	1	0.75	3.295	3835.969	0.088	100
	Phenol, 2-methyl-5-(1-methylethyl)-	150.22	391.905	1	0.75	3.293	3709.313	0.075	100
	Caryophyllene	204.355	449.878	0	0	5.037	9906.038	1.033	100
	Humulene	204.355	455.531	0	0	5.133	9906.038	1.044	100
	1H-Cycloprop[e]azulen-4-ol, decahydro-1,1,4,7-tetramethyl-, [1aR-(1aalpha,4beta,4abeta,7alpha,7abeta,7balpha)]-	222.37	458.88	1	0.75	3.9	5183.091	0.274	100
ROMEO	Benzofran-3-one, 2-[3,4-dihydroxybenzylidene]-6-hydroxy-	270.241	436.668	1	4.25	0.468	264.36	− 1.21	73.036
	9,12,15-Octadecatrienoic acid, (Z,Z,Z)-	278.434	640.559	1	2.75	3.96	1384.156	− 0.507	100
	9,12-Octadecadienoic acid (Z,Z)-	280.45	641.478	1	2.75	3.987	1384.156	− 0.504	100
	Ethanol, 2-(9-octadecenyloxy)-, (Z)-	312.535	759.057	2	2	5.474	3614.04	− 0.023	100
	n-Hexadecanoic acid	256.428	696.398	1	2.75	4.184	1384.156	− 0.636	100
	1,6-Dioxaspiro [4.4]non-3-ene, 2-(2,4-hexadiynylidene)-	200.237	346.979	0	3	1.134	9906.038	− 0.623	100
	Tetrahydropyranylethyleneglycol	146.186	307.629	3	3	− 0.077	1773.706	− 0.098	71.682
	Verbenone	150.22	423.127	0	0.75	2.862	3864.033	0.101	100
	n-Propyl 9,12-octadecadienoate	322.53	709.539	0	3	5.24	5399.804	0.238	100
	4H-Pyran-4-one, 2,3-dihydro-3,5-dihydroxy-6-methyl-	144.127	342.706	1	3.75	− 0.254	905.191	-0.603	78.38

Table 6. ADMET prediction. mol MW: mass of molecules (acceptable range: 500 mol). SASA: Total solvent accessible surface area using a probe with a 1.4 radius (acceptable range: 300–1000radius). donorHB: Donor of hydrogen bonds (acceptable range: ≤ 5). accptHB: Acceptor of hydrogen bonds (acceptable range: ≤ 10). QPlogPo/w: Predicted octanol/water partition coefficient (acceptable range: − 2 –6.5). QPPCaco: Predicted apparent Caco-2 cell permeability in nm/s. Caco-2 cells is a model for the gut-blood barrier (˂25-poor, ˃500-great). QPlogBB: Predicted blood–brain partition coefficient (acceptable range: − 3 –1.2). %HOA: Predicted human oral absorption on 0 to 100% scale (< 25% is poor, and > 80% is high).

pharmacological characteristics of the monoterpene *p*-cymene, such as its antiviral, anticancer, antibacterial, antifungal, antioxidant, and antiparasitic effects, have been demonstrated in several studies[27]. In addition, *p*-cymene has been shown to *p*-cymene function as a neuroprotective, immunomodulatory, analgesic, and antinociceptive agent. Certain mechanisms, including apoptosis and cell cycle arrest prevention, are associated with its anticancer effects[28].

Phenolic compounds are plant constituents with an aromatic ring featuring one or more hydroxyl groups. Approximately 8000 naturally occurring plant phenolics have been identified. Among these constituents are flavonoids, which represent a significant category of naturally occurring phenolic substances, existing both in their unbound form and as glycosides. Among the various subclasses of phenolics, flavonoids represent the most abundant and diverse category of phenolic compounds present in nature. These compounds exist in both free and glycoside forms across a range of plant tissues. The contribution of flavonoids to the enhancement of TPC and antioxidant potential in plants is illustrated by their occurrence in multiple plant structures[29]. *R. officinalis* is a rich source of phenolic compounds, and its properties are derived from its extracts and EOs. Both methods have been applied to medical conditions[30]. The measurements of total phenolic content (TPC) and total flavonoid content (TFC) for ROLEO and ROLMEdisclose vital information about their phytochemical attributes and potential bioactive functions. Using the Folin-Ciocalteu method, TPC for ROLEO was determined to be 49.34 ± 2.84 GAE/g dry weight of the dry while ROLME showed a TPC of 38.13 ± 3.31 GAE/g dry weight of the dry extract. Similarly, the $AlCl_3$ assays indicated values of 24 ± 1.47 mg QE/g dry weight of the dry extract for ROLEO and 19 ± 1.47 mg QE/g dry weight of the dry extract for ROLME. These results indicate that ROLEO is rich in phenolic and flavonoid compounds, reinforcing its potential as a natural source of antioxidants. However, contrary findings have been reported in the literature. A recent study showed that ROLME exhibited a higher TPC of 127.1 ± 2.40 µg GAE/mg extract compared to ROLEO, which has a TPC of 7.81 ± 0.41 µg GAE/g extract. Additionally, the TFC for ROLME was reported as 38.61 ± 0.75 µg QE/mg extract, while ROLEO exhibited a TFC of only 0.01 ± 0.00 µg QE/mg extract[19]. The concentration of these chemicals in the final extract is directly affected by both the intrinsic characteristics of the plants and external influences, such as pre-extraction processing and extraction conditions[31,32]. In various solvent extractions, the TPC value of rosemary leaves was 72.34 ± 4.9 GAE mg/g for ethanol extraction, 64.44 ± 6.6 GAE mg/g for methanol, 57.74 ± 7.9 GAE mg/g for acetone, 52.04 ± 3.8 GAE mg/g for ethyl acetate, 48.94 ± 5.5 GAE mg/g for water, 37.34 ± 6.9 GAE mg/g for diethyl ether, and EOs (9.9 ± 0.06 GAE mg/g)[33]. The TPC and TFC yields of *R. officinalis* aerial parts (flowering tops) methanol extract

were 34.72 ± 1.65 mg GAE/g DM), and TFC (25.02 ± 1.53 mg QE/g DM, respectively[34]. The amount of (poly) phenolic chemicals in an acetone extract of dry rosemary leaves was 166.32 ± 11.05 mg/mL[35]. The chemical structure and redox characteristics of phenolic compounds enable them to function as hydrogen donors and reducing agents for transitional metals, scavenge free radicals, and inhibit lipoxygenase, which are the primary mechanisms underlying their antioxidant action[36].

The DPPH and ABTS methods are the most commonly employed techniques for assessing antioxidant capacity, owing to their simplicity, rapidity, sensitivity, and the utilization of stable radicals[37]. The current findings indicated that ROLEO had a lower IC_{50} value (93.41 ± 17.15 µg/mL) and hence stronger antioxidant activity than ROLME, which had an IC_{50} value of 172.42 ± 1.24 µg/mL. Similarly, regarding the ABTS assay, the IC_{50} values for ROLEO and ROLME were 90.71 ± 2.15 µg/mL and 163.11 ± 2.12 µg/mL, respectively. Our findings agree with those of a previous study that reported that rosemary EO displayed a strong radical scavenging activity with IC_{50} values (3.53 ± 0.038 µL/mL) compared to that of the methanol extract, with IC_{50} values (11.741 ± 0.004 µg/mL)[38]. An early study revealed that the aerial parts of ROLEO have in vitro antioxidant activity and a comparatively significant ability to scavenge DPPH radicals, with an IC_{50} value of 77.6 µl/mL[23]. The ethanol extract of rosemary leaves had IC_{50} values of 40.76 ± 2.81 µg/mL for the DPPH assay and 70 ± 4.67 µg/mL for the ABTS technique[39]. The lower IC_{50} value for ABTS in the ROLEO may indicate that ROLEO includes chemicals more effective in hydrogen donation than electron donation. The modest antioxidant activity of ROLEO can also be linked to the bioactive components discovered during GC–MS research, such as phenol, 2-methyl-5-(1-methylethyl), and p-Cymene, which have been shown to have antioxidant characteristics, contribute to the free radical scavenging activity demonstrated in this study. The mechanisms of action of these chemicals have been thoroughly investigated. Recent studies have indicated that the antioxidant activity of rosemary is attributable to its richness in isoprenoid quinones, which function as chain terminators of free radicals and chelators of reactive oxygen species (ROS)[40]. The phenolic compounds in the commercial rosemary extracts operate as the main antioxidants when interacting with lipid and hydroxyl radicals to transform them into stable products[41]. The methodologies used by DPPH and ABTS assays to test antioxidant activity were different. The DPPH assay relies on reducing a methanolic DPPH solution when an antioxidant donates hydrogen during the reaction, resulting in the formation of the non-radical form DPPH-H. The extract demonstrated the capability to convert the stable radical DPPH into the yellow-hued di-phenylpicrylhydrazine[42]. The ABTS radical cation method involves the generation of a nitrogen-centered synthetic radical cation through the oxidation of ABTS using potassium persulfate. An antioxidant component can donate an electron to convert the ABTS radical dot into its non-radical state[43].

The MTT assay was used to examine the toxicity of ROLEO and ROLME in the human cancer cell lines MCF-7 and HepG2. The results indicate that ROLEO exhibited higher efficacy than ROLME in both the tested MCF-7 and HepG2 cells, with IC_{50} values of 156.12 ± 0.94 µg/mL in MCF-7 and 125.82 ± 2.14 µg/mL in HepG2, respectively. These findings indicate that ROLEO has a strong anticancer effectiveness, particularly in comparison to the positive control, cisplatin (30 µg/mL). In MCF-10A cells, the ROLEO or ROLME showed a slight effect on cell viability where cell viability was above 80%. The findings were consistent with an earlier study on Dorycnium pentaphyllum extract, which showed cell viability remained above 80%.On the other hand, no toxic effect was observed in MCF-12A cells after 48 and 72 h exposure to the extract[44]. Human mammary epithelial cell lines, such as MCF-10A, a non-malignant cells, are widely used as model systems in toxicology studies[45], due to their morphological resemplance to normal, normal human mammary epithelial cells[45]. Similar to tumorigenic (MCF7), both non-tumorigenic (MCF 10A, MCF-12A) cells are both estrogen receptor-positive and progesterone receptor-positive[46]. However, MCF-12A is notably difficult to culture, making MCF-10A a more practical choice for representing normal human mammary epithelial cells in this study.

Currently, cisplatin is the preferred treatment for various cancers, including testicular, ovarian, bladder, prostate, cervical, and lung cancers. Cisplatin functions as an anticancer agent through several mechanisms. Its primary actions, which ultimately lead to cell death, include activating various signal transduction pathways, modulating different genes, and forming DNA–platinum adducts by interacting with purine bases. However, the side effects associated with cisplatin and the development of drug resistance are significant obstacles that hinder its use and effectiveness. Its interaction with glutathione and metallothioneins reduces its accumulation in cancer cells and promotes the repair of DNA lesions, which contributes to the resistance observed with cisplatin[47]. ROLEO showed stronger activity against HepG2 cells compared to MCF-7 cells, indicated by a lower IC_{50} value. This may be related to its diverse phytochemical composition, particularly the presence of bioactive compounds. These compounds are recognized for their anticancer effects, which include reducing cancer cell growth, inducing apoptosis, and inhibiting angiogenesis. Similar findings have been reported in previous studies on the to cytotoxic effects of the rosemary extract on several cell lines. For instance, a preliminary examination showed that the ROLEO had an activity of 508.7 µg/ml against HepG2 cells and 525.7 µg/ml against ECV304 cells[48]. Another study revealed that the ROLEO exhibited the most significant cytotoxicity against SK-OV-3, HO-8910, and Bel-7402 cancer cells in comparison to its constituents, which include 1,8-cineole, α-pinene, and β-pinene. The IC_{50} values for the cancer cell lines treated with ROLEO were found to be 0.025‰, 0.076%, and 0.13‰ (v/v), respectively[49]. An early examination showed that crude ethanolic rosemary extract was effective in diminishing the growth of breast cancer cells, particularly in the MCF-7 (ER+) and MDA-MB-468 (TN) cell lines, with IC_{50} values of 90 µg/mL and 26.8 µg/mL, respectively[50]. Further studies have demonstrated that ROLEO was moderately cytotoxic to MCF-7 cells at a concentration of 800 µg/ml (IC_{50} = 47.39 ± 0.91)[51]. Đilas et al. (2012) reported that rosemary extracts had a significant antiproliferative effect ($P \leq 0.01$) on cervix epitheloid carcinoma (HeLa), with an IC_{50} of 10.02 µg/mL, and on MCF-7, with an IC_{50} of 9.95 µg/mL[52]. Similarly, extracts of *R. officinalis* from Yemen showed marked cytotoxicity against two cancer cell lines, 5637 and MCF-7, with IC_{50} values lower than 50 µg/mL[53]. These findings highlight the potential use of ROLEO as a natural anticancer drug.

Apoptosis serves as the crucial mechanism for maintaining equilibrium between cellular proliferation and growth, thereby averting the risk of uncontrolled malignancy. Many anticancer agents facilitate the elimination of cancer cells by exploiting intact apoptotic signaling pathways[54]. The ability of ROLEO and ROLME to trigger apoptosis in MCF-7 and HepG2 cells was examined through RT-qPCR, which demonstrated significant alterations in both pro-apoptotic and anti-apoptotic gene expression. ROLEO and ROLME treatment increased apoptotic genes (*caspase-3*, *-8*, *-9*, and *Bax*) and decreased anti-apoptotic genes compared to untreated control cells. The elevation of caspases following exposure to ROLEO and ROLME suggests that the extract induces apoptosis mediated by caspases, leading to the demise of cancer cells. This illustrates that the apoptotic process induced by both therapies in cancer cells contributes to their deadly consequences[55,56]. EOs are known to suppress cell proliferation through various mechanism such as depolarization, increased membrane permeability, decreased activity of enzymes confined to the membrane, and induction of apoptosis [57]. A previous study revealed that an ethanolic extract of *R. officinalis* at a concentration of 300 µg/mL stimulated the activation of caspase-3 and caspase-7 in the MG-63 human osteosarcoma cell line[58]. The primary phenolic ingredient in rosemary, rosmarinic acid, prevented the development of tumor spheroids and colony formation and decreased cell proliferation in a cell viability study.

Furthermore, rosmarinic acid increased apoptosis in PC-3 and DU145 cells by modulating the expression of genes related to the intrinsic mitochondrial apoptotic pathway, including Bax, Bcl-2, caspase-3, and poly (ADP-ribose) polymerase 1 (PARP-1) (cleaved). This was achieved by upregulating p53, which is derived from HDAC2 downregulation[59]. Our results support these findings, indicating that ROLEO and ROLME promote apoptosis in a dose-dependent manner by activating key apoptotic pathways, as evidenced by the increased expression of caspase-3, -8, -9, and Bax.The induction of apoptosis occurs through three main mechanisms: extrinsic pathways mediated by death receptors, intrinsic pathways involving mitochondria, and endoplasmic reticulum stress-(ERS)- dependent pathways which contribute to cell death signaling[60]. He activation of executioner caspases-3, -6, and -7 is significantly facilitated by caspase-8, which is a key component of the extrinsic pathway leading to apoptosis. In the context of the intrinsic pathway, caspases -3 and -7 are critical upstream mediators that initiate the apoptotic process. Studies have revealed that caspase-3 possesses both endogenous and exogenous apoptotic properties through its interactions with caspases-8 and -9[60]. Anti-apoptotic genes, including Bcl2, inhibit apoptosis by maintaining the integrity of the mitochondrial membrane. Consequently, the ratio of Bax to Bcl2 is critical in determining sensitivity to apoptotic signals. The reduction of anti-apoptotic gene expression in both MCF-7 and HepG2 cell lines supports the hypothesis that ROLEO and ROLME interfere with the survival mechanisms of cancer cells, thereby increasing their susceptibility to apoptotic stimuli. The regulation of these pathways serves as an essential therapeutic technique in cancer management, as many cancer cells can resist apoptosis due to the overexpression of anti-apoptotic proteins, particularly Bcl-2[61]. The findings indicate the potential therapeutic significance of ROLEO in cancer treatment, particularly as a natural anticancer agent that facilitates caspase-mediated apoptosis.

Numerous plants with enzyme-inhibiting properties have been investigated for their potential in diabetes treatment. Researchers are actively exploring new intestinal α-glucosidase and pancreatic α-amylase inhibitors derived from, plants that exhibit hypoglycemic effects with minimal to no adverse side effects[62]. The current study found that ROLEO had the best antidiabetic activity to inhibit α-amylase and α-glucosidase (IC_{50} values of 174 ± 2.14 µg/mL and 156.62 ± 1.23 µg/mL, respectively), in comparison to ROLME, which had IC_{50} values of 243 ± 0.24 µg/mL and α-glucosidase (IC_{50} = 216.62 ± 0.22 µg/mL). In agreement with our findings, a recent in vitro investigation found that the ROLEO had higher α-amylase inhibitory activity (26.29%) than acarbose (positive control), which showed (4.55%) inhibition[63]. Another study showed that the rosmarinic acid extract (8.88 mM) was also demonstrated to inhibit α-amylase activity significantly[64]. Interestingly, Kabubii et al. (2024) reported that the aqueous extract of *R. officinalis* leaves significantly reduced glucose levels in streptozotocin-induced diabetic Wistar rat model[8]. Further investigation revealed that the ethanolic leaf extract of *R. officinalis* effectively lowered blood glucose levels in rabbits with normoglycemia, glucose hyperglycemia, and alloxan-induced diabetes[65]. These findings are important because they support the long-standing practice of using *R. officinalis* to treat various diseases, including metabolic disorders. These inhibitory effects may be attributed to the presence of bioactive chemicals such as phenolics and flavonoids.

The rise of antimicrobial resistance represents a critical public health issue affecting populations worldwide, as a growing number of pathogenic organisms, including bacteria and fungi increasingly have developed resistance to one or more antimicrobial medications, collectively known as multi-resistant organisms. In the past decade, extensive endeavors have been undertaken to investigate natural products from a variety of sources, including plants, environments, and microorganisms. For thousands of years, these products have proven to be an essential and beneficial source of anticancer and antimicrobial agents. Antimicrobial compounds derived from medicinal plants possess the potential to inhibit the growth of bacteria, fungi, viruses, and protozoa through mechanisms distinct from those utilized by conventional antimicrobials. Furthermore, they may offer considerable clinical advantages in addressing microbial strains that resist existing antimicrobial therapy[66]. The findings of the current study demonstrate that ROLEO (MIC values = 4.68 ± 2.21—25 ± 0.00 µg/mL) exhibits greater antibacterial activity compared to ROLME (MIC values = 12.50 ± 0.00—25 ± 0.00 µg/mL) against all tested bacteria, with a notable efficacy against Gram-positive bacteria. These findings are consistent with an earlier investigation that found that the tested bacteria were partly responsive to the methanolic extracts and sensitive to the ROLEO. Especially Notably, *Proteus vulgaris* and *Enterococcus faecalis* were the most susceptible to the essential oil.[67]. In contrast, a recent study on the antibacterial activity of ROLEO and ROLME in Egypt reported that only ROLME showed inhibitory effects against Gram-positive bacteria and pathogenic yeast but not ROLEO[68]. ROLME also inhibited the growth of *P. aeruginosa*, *E. coli*, and S. *aureus*, with *P. aeruginosa* exhibiting the highest sensitivity to ROLME, with a 19.8 mm growth inhibition zone, and *S. aureus* exhibited the lowest sensitivity, with a 14.4 mm growth inhibition zone[69]. The synergistic interaction of *R. officinalis*

components disrupts the bacterial cell membrane to influence electron transfer, fatty acid transport, genetic material production, and cellular component leakage[70]. Protein interactions with the membrane also cause loss of membrane structure and function. These differences in the susceptibility between Gram-positive and Gram-negative may be due to differences in cell membrane permeability or other genetic factors[71]. Furthermore, a combination of less common compounds found in ROLEO or most of the compounds may be the primary cause of antibacterial activity.

The molecular docking investigations of the bioactive compounds in ROLEO and ROLME yield valuable insights into their antioxidant, antibacterial, antidiabetic, and anticancer activities. *In-silico* studies revealed glide scores, which measure the binding affinity between a ligand and a receptor, is an essential parameter to predict molecular affinity. The lower the glide score (i.e., the more negative it is), the stronger the ligand and receptor interaction. This indicates an optimal stabilization of the ligand-receptor complex through noncovalent interactions such as hydrogen bonds, hydrophobic, and electrostatic interactions[72]. The molecules identified in ROLEO (1H-Cycloprop[e]azulen-4-ol, Thymol, and Phenol, 2-methyl-5-(1-methylethyl)-) and ROMEO (Benzofran-3-one, Bisabolol oxide B, and Verbenone) show glide scores ranging from − 5.043 to − 6.149 kcal/mol against α-amylase. These scores indicate a significant affinity for inhibiting this key enzyme involved in the digestion of complex carbohydrates. By inhibiting α-amylase, these compounds may help reduce postprandial glucose spikes, a central goal in the management of type 2 diabetes[73]. Regarding anticancer activity, the compounds identified in ROLEO (Thymol, Bicyclo[3.1.0]hexan-3-one, and Phenol, 2-methyl-5-(1-methylethyl)-) and in ROMEO (4H-Pyran-4-one, Benzofran-3-one, and Verbenone) exhibit glide scores ranging from − 4.680 to − 5.989 kcal/mol against caspase-3. Inhibition of this enzyme, which plays a crucial role in apoptosis, could prevent cancer cells from exploiting apoptotic pathways to avoid programmed cell death[74]. The results also reveal a strong antibacterial activity of ROLEO and ROMEO compounds against *E. coli* gyrase B, an essential enzyme in bacterial DNA replication. Molecules such as Thymol, Benzofran-3-one, and 1,6-Dioxaspiro[4.4] non-3-ene show glide scores ranging from − 5.573 to − 7.231 kcal/mol, indicating a high affinity for this target. These results are consistent with previous studies demonstrating the efficacy of gyrase B inhibitors as promising antibacterial agents[75].

The interactions and types of bonds between the ligands and the different active sites, such as hydrogen bonds, pi-cation interactions, and pi-pi stacking, play a crucial role in stabilizing ligand-target complexes. These interactions determine the binding affinity and specificity of bioactive molecules, influencing their therapeutic potential.

Hydrogen bonds strengthen ligand-target affinity by providing directional electrostatic interactions, stabilizing the complex within the active site. These are essential for enzyme inhibitors as they help anchor the ligand to key residues[76]. Pi-cation interactions involving a positive charge and an aromatic system contribute strong electrostatic forces that stabilize complexes in catalytic pockets[77]. Pi-pi stacking stabilizes hydrophobic and aromatic interactions, enhancing ligand specificity for their targets[78]. Together with salt bridges, these interactions are crucial for modulating enzymatic activity and disrupting pathological pathways[79].

ADMET parameters are critical in evaluating a molecule's pharmacokinetic behavior and therapeutic potential. Molecules with favorable molar mass (< 500 g/mol), such as thymol (150.22 g/mol), ensure better absorption and permeability[80]. High Caco-2 cell permeability, like that of thymol (3835.969 nm/s), indicates excellent intestinal absorption[81]. Moreover, high oral bioavailability (100% for ROLEO molecules) ensures efficient drug delivery.

While this study provides valuable insights, it is essential to acknowledge certain limitations that can inform and guide future research efforts. For instance, further investigations are needed to compare the different fractions derived from the samples, as well as to analyse their phytochemical composition and biological activity. To validate the recently identified compounds, the retention indices of the components were calculated using linear interpolation concerning the retention durations of two common n-alkane mixes (C_8–C_{20} and C_{21}–C_{40}). Additionally, techniques such as liquid chromatography-mass spectrometry (LC–MS) and high-performance liquid chromatography (HPLC) are needed to identify and quantify specific polyphenols. Furthermore, the lack of in vivo research creates a gap in our understanding of targeted organ delivery, efficacy, and potential side effects in more complex physiological conditions. Future research should prioritize in vivo studies to determine the effectiveness and safety of these substances.

In conclusion, GC–MS analysis of ROLME revealed 20 bioactive compounds, some of which were unique, whereas GC–MS analysis of ROLEO revealed 73 bioactive compounds. Compared to ROLME, ROLEO has higher antioxidant activity at low concentrations, antidiabetic properties via inhibition of α-amylase and α-glucosidase enzymes, potential lower-dose anticancer effects, and antibacterial activities, particularly against Gram-positive bacteria. Overall, this study highlights the broad range of applications of ROLEO and ROLME as anticancer, antidiabetic, and antioxidant agents. Research on the mechanisms of action and potential therapeutic uses of these chemicals, both alone and in combination, is necessary in light of the identified bioactivities. In vivo investigations will be the main focus of future studies to evaluate the efficacy and safety of these compounds.

Materials and methods

Plant material and preparation

The *R. officinalis* was commercially obtained from a local market in Riyadh, Saudi Arabia in August of 2024. *R. officinalis* is a bushy, evergreen plant. Upright spikes of fragrant, dark green leaves and purple-blue blooms from mid-spring to early summer. The selected plant species were validated by Prof. Dr. Mohammed Fasil, and voucher specimens were deposited in the herbarium of the Department of Botany and Microbiology, College of Science, King Saud University, Riyadh, Saudi Arabia (KSU NO-19897). However, the collection of plant materials was conducted following the guidelines of the International Union for Conservation of Nature (IUCN)

policies research involving species at risk of extinction and the Convention on the Trade in Endangered Species of Wild Fauna and Flora.

The *R. officinalis* was carefully washed with running water to remove surface impurities. They were then allowed to dry for 10 days at room temperature. As previously mentioned[19], ROLEO extraction was performed by hydrodiztilling 100 g of dried and ground *R. officinalis* leaves and branches for three hours with 1000 mL of distilled water using a Clevenger-style device. Following collection and drying on anhydrous sodium sulfate, the extracted ROLEO was stored in sealed glass vials at − 4 °C until needed.

ROLME was performed using methanol as described previously by[19]. Fifty grams of leaf powder were extracted by dissolving it in 500 ml of methanol: water (80:20, v/v). This allowed for the extraction of the desired compounds from the plant material. The mixture was shaken overnight at 100 rpm at room temperature. After the extraction phase, contaminants or solid residues were eliminated from the extracts using the Whatman No. 1 filter paper. The extracts were dried using vacuum-assisted drying by exposing them to a temperature of 30 °C. The produced dried extracts were then stored in a refrigerator at 4 °C until further use.

Identification of bioactive compounds

GC–MS system Agilent 7890B coupled to Agilent 5977A MSD equipped with a single quadrupole mass analyzer capillary HP-5MS UI (Ultra Inert), length: 30 m, i.d.:0.25 mm, film thickness: 0.25 µm, stationary phase: 5% phenyl, methylpolysiloxane (low polar) from Agilent Technologies (Santa Clara, CA, USA) was employed to identify the bioactive components. The temperature was set to be at 50 °C for three minutes, 280 °C for 15 min, 250 °C for one minute, and 7.5 °C/min constant. A liquid delay of 4 min, acquisition scan type, a mass range of 50–1000 Da g/mol, and a scan speed of 1.56 u/sec. The carrier gas (helium) was maintained at a constant 1 ml/min flow rate. The results were collected from the GC–MS at an ionization voltage of 70 eV in EI ionization mode. The temperatures of the injector and detector were set at 250 °C and 300 °C, respectively.

The search library used was Willey and the National Institute of Standards and Technology (NIST) mass spectral database. By comparing the components with those found in the NIST computer libraries connected to the GC–MS equipment, parts with a matching factor greater than 90% were identified.

Determination of TPC and TFC

TPC was determined using the Folin-Ciocalteu method as described in an early study[82]. TPC was calculated using a standard curve created from the gallic acid standard (10–100 mg/mL). Following the designated concentration of the extract, a mixture was prepared by combining 0.25 mL of the extract with 1.25 mL of the Folin–Ciocalteu reagent (phosphomolybdate and phosphotungstate), in addition to 7.5% $NaHCO_3$. This mixture was incubated at 45 °C for 15 min, and then the absorbance at 765 nm was measured using a spectrophotometer (U2001 UV–vis Spectrophotometer, Hitachi, Japan). The linearity of the curve was assessed using the coefficient of determination (R^2) of calibration curves. Gallic acid equivalent (mg GAE)/g of extract was used to express the findings.

TFC was determined using the aluminum chloride ($AlCl_3$) colorimetric method, as described in a previous study[83]. In this method, approximately 0.1 mL of the extracts were separately incubated with 2.0 mL of a 2% $AlCl_3$ solution and 1.0 M sodium acetate for 30 min at room temperature. Following incubation, the absorbance of the extract was measured using a spectrophotometer (U2001 UV–vis Spectrophotometer, Hitachi, Japan) at a wavelength of 420 nm. A standard curve with quercetin concentrations ranging from 0 to 100 mg/mL was created to quantify TFC. TFC is expressed as mg quercetin equivalent mg (QAE) + /g of the extract.

Antioxidant activity

DPPH assay

Using the previously mentioned methodology[84], the DPPH radical scavenging assay was used to evaluate the ROLEO and ROLME capacities to react with DPPH radicals. The extracts were prepared at five concentrations (50, 100, 200, 400, and 800 µg/mL). For each concentration, approximately 0.5 mL of the extract was mixed with 0.375 mL of methanol and a DPPH solution (2 mL, 0.08 mM). The reaction mixture was then placed in a dark environment and incubated for 30 min. After incubation, the optical density (OD) of the mixture was measured at 517 nm using a spectrophotometer (U2001 UV–vis Spectrophotometer, Hitachi, Japan). Ascorbic acid was used as a positive control at known concentrations (400 µg/mL). The proportion of DPPH scavenging activity (%) was determined using the following equation: DPPH radical scavenging activity [%] = [(Ac—A)/Ac] × 100, where Ac denotes the absorbance of the control, and A denotes the absorbance of the sample. The half-maximal inhibitory concentration (IC_{50}) value was computed using Graph Pad Prism software (version 5.0, La Jolla, CA, USA). The IC_{50} of DPPH scavenging activity was determined graphically using the line equation obtained from the % value of the antioxidant activity and the concentration value plotted on a graph, where the concentration value is on the *X*-axis, and the % activity is on the *Y*-axis[85].

ABTS assay

The ABTS radical scavenging assay was conducted using the methodology outlined in previous study[86]. Ascorbic acid (200 µL, 400 µg/mL) was used as the positive control. The assay was carried out by first mixing the ABTS solution (192 mg/50 ml) with the $K_2S_2O_8$ solution (140 mM). Consequently, the reaction mixture was placed in the dark at room temperature for about 12 h. In addition, the ABTS solution was mixed with methanol to achieve an OD of 0.70 ± 0.02 at 734 nm. Furthermore, fifty microliters of each extract concentration were thoroughly mixed with 3 mL of diluted ABTS. Moreover, the mixture was incubated for 6 min in dark conditions. Subsequently, the OD was measured at 734 nm using a spectrophotometer ((U2001 UV–vis Spectrophotometer, Hitachi, Japan). The results are presented as IC_{50} and ABTS % values, as described above.

Cell culture and cytotoxicity assays

This study investigated the toxic properties of various plant extracts using several cell lines: human hepatoma HepG2 (ATCC HB-8065), breast cancer MCF-7 (ATCC HTB-22), and the normal human epithelial breast cell line MCF-10A (ATCC CRL-10317), which serves as a non-tumorigenic epithelial model system in vitro. The cells were cultured in Dulbecco's Modified Eagle Medium (DMEM), supplemented with 1% penicillin–streptomycin and fetal calf serum (FCS). The Cells were cultured at 37 °C in a 5% CO_2 humidified environment. Cell viability was determined using a 3-(4,5-dimethylthiazol-2-yl)-2,5-diphenyl-2H-tetrazolium bromide (MTT) test. The principle of the MTT assay is that mitochondria reduce yellowish MTT to create purple formazan granules[87]. One hundred milliliters of DMEM (100 mL) were added to each well of the 96-well microplate for inoculation, by incubating the microplate for 24 h at 37 °C, 95% humidity, and 5% CO_2, a completely formed monolayer sheet was created. Serial dilutions of 0.1% dimethyl sulfoxide (DMSO)-solubilized extracts were prepared using a growth medium at 50–400 µg/ml. The Cells treated with the extract were then incubated for 24 h at 37 °C and 5% CO_2. Cisplatin (30 µg/mL) was used as a positive control. Negative control cells were incubated without the addition of stem and leaf extracts. Next, 10 µL MTT solution was added to each well. A shaker (MPS-1, Biosan, London, UK) was used for mixing, and it was run for five minutes at 150 rpm. The incubation was continued for 4 h. Formazan, a metabolic byproduct of the MTT assay, was resuspended in 100 µL of DMSO and vigorously shaken at 150 rpm for five minutes. The optical density at 570 nm was measured using an ELX-808 microplate reader (BioTek Laboratories, LL, Shoreline, W.A, USA). Data were corrected using a background reference wavelength of 620 nm. Once cell viability (%) was established, an experiment was performed in triplicate. Graph Pad Prism software (version 5.0, La Jolla, CA, USA) was used to calculate the IC_{50} value after the mean value ± SD was considered for data processing[88].

RT-PCR assay of apoptosis genes and Morphological observations

RT-PCR was used to assess the expression of anti-apoptotic (*Bcl-xL* and *Bcl-2*) and apoptotic genes (*caspase-3*, *8*, *9*, and *Bax*). Additionally, an inverted microscope (Eclipse TS100, Nikon, Japan) was used to observe the morphological changes induced by ROLEO and ROLME on MCF-7, HepG2, and MCF-10A cells. MCF-7, HepG2, and MCF-10A cells. MCF-7, HepG2, and MCF-10A cells (2×10^3 cells) were collected and put in six-well plates with 100 µg/ml of the plant 1extract. After centrifugation at 500 g for 5 min at 4 °C, the pellet was used for RNA extraction using an RNeasy kit (Qiagen, Hilden, Germany), and the supernatant was removed. This RNA served as the template for RT-PCR. The RT-PCR reactions were performed in a 7500 Fast real-time PCR (7500 Fast; Applied Biosystems, Foster City, CA, USA). The RT-qPCR methodology is described in our recent study[89].

Antidiabetic activity

In vitro α-amylase inhibition assay

A 3,5-dinitrosalicylic acid (DNSA) assay was used to ascertain the inhibition of α-amylase activity, as previously reported[90]. Briefly, plant extracts were diluted to reach concentrations ranging from 50 to 1000 µg/mL using the buffer (0.02 M Na2HPO4/NaH2PO4; 0.006 M NaCl; pH 6.9). The mixture was incubated for 10 min at 37 °C after 200 µL of each extract and 200 µL of the Molychem α-amylase solution (2 units/mL) were mixed. Each tube was then filled with 200 µL of the 1% starch solution (w/v), and the tubes were left for 3 min at 37 °C. In total, 200 µL of DNSA reagent (12 g of sodium potassium tartrate tetrahydrate in 8.0 mL of 2 M NaOH and 20 mL of 96 mM 3,5-DNSA solution was added to stop the reaction, and it was then heated for 10 min at 85 °C in a water bath. The positive control was 100 µL of 400 µg/mL of acarbose (Bayer). After allowing the sample to cool to room temperature and diluting it with 5 mL of distilled water, the OD at 540 nm was measured using a UV–visible spectrophotometer (U2001 UV–vis Spectrophotometer, Hitachi). α-Amylase inhibition was calculated and expressed as a percentage of inhibition, and IC_{50} values were calculated using Graph Pad Prism software (version 5.0, La Jolla, CA, USA).

In vitro α-glucosidase inhibition assay

As previously reported[91], yeast α-glucosidase and p-nitrophenyl-α-D-glucopyranoside (pNPG) were used to assess the α-glucosidase inhibitory activity. The extracts (100 µL, 20 mg/mL) or 400 µg/mL of acarbose (serving as a positive control) were mixed with 50 µL of α-glucosidase (1 U/mL) produced in 0.1 M phosphate buffer (pH 6.9) and 250 µL of 0.1 M phosphate buffer to reach a final concentration of 0.5 to 5.0 mg/mL. The mixture was incubated for 20 min at 37 °C. Subsequently, 10 µL of 10 mM pNPG produced in a 0.1 M phosphate buffer (pH 6.9) was added, and the mixture was incubated for one hour at 37 °C. The OD was measured at 405 nm using a spectrophotometer (U2001 UV–vis Spectrophotometer, Hitachi, Japan) after the reactions were stopped by adding 650 µL of 1 M sodium carbonate. The results were represented as a percentage of the enzyme activity inhibition (%), and IC_{50} values were calculated using GraphPad Prism.

Antibacterial activity

Disc diffusion assay

The antibacterial activities of ROLEO and ROLME were determined using the disc diffusion method, as previously indicated[92]. The microbial strains used in this study were Gram-positive bacteria (*Staphylococcus aureus*, ATCC -23,235; *Staphylococcus epidermidis,* ATCC-12228; *Bacillus subtilis*, ATCC- 23,857) and Gram-negative bacteria (*Escherichia coli* ATCC-25922; *Pseudomonas aeruginosa*, ATCC-27853; *Klebsiella pneumonia* ATCC-13883). A mixture of 100 µL suspensions, including 10^7 CFU/mL of bacteria in the exponential growth phase, was spread over Mueller–Hinton agar medium (HMA). The next step included incubating petri dishes at 37 °C for 24 h. Hole-punching with a 5 mm diameter cork-borer was used to create wells at equal surface intervals. The plant extracts (100, 200, 400, and 800 µg/ml; 100 µL/well) were mixed with the resulting wells in triplicate and placed on inoculated Petri plates. Chloramphenicol (25 µg/ml) was used as the positive control,

whereas Muller Hinton Broth (HMB) with 0.1% DMSO was used as the negative control. The Petri dishes were incubated at 37 °C for 24 h. Measuring the inhibition zone (mm) against the microorganisms under study, including the disc diameter, allowed the evaluation of antibacterial efficacy.

Minimum inhibitory/bactericidal concentration (MIC/MBC)

The broth dilution technique determined the MIC and MBC of ROLEO and ROLME using the 2,3,5-triphenyl tetrazolium chloride (TTC) method[93] with some modifications. First, a pathogenic bacterial primary culture was prepared at 5×10^6 CFU/ml. Subsequently, 1.95–1000 µg/ml extract was diluted with MHB. One hundred microliters of the extract were applied to each well of a 96-well plate, and bacteria were added. The plates were incubated for 24 h at 37 °C. After adding 20 µL (2 mg/mL) of TTC to each well, the growth of microorganisms was observed by observing the formation of a crimson color. No color change was observed at a concentration known to be the minimum color (MIC). One hundred microliters of content from each well that did not change in color were cultured on MHA and incubated at 37 °C for 24 h. The smallest dilution that inhibited growth[94].

Molecular docking

Molecular docking was applied to conduct a theoretical evaluation of the potential antidiabetic, anticancer, and antibacterial effects associated with ROLEO and ROLME.

Ligand preparation

The process of preparing ligands commenced with obtaining the compounds from ROLEO and ROLME in SDF format via the PubChem database. Using Schrödinger's LigPrep module (version 11.5), these ligands were refined and optimized under the OPLS3 force field. Adjustments were made to account for ionization states at a physiological pH range of 7.0 ± 2.0, enabling the generation of up to 32 stereoisomeric forms for each compound[95].

Protein preparation

Proteins used in the docking study were sourced from the Protein Data Bank, including human α-amylase (PDB ID: 1B2Y)[96], caspase 3 (PDB ID: 3GJQ)[74], and *E. coli* gyrase B (PDB ID: 3G7E)[97]. The preparation process involved refining their structures by adding hydrogen atoms, correcting bond orders, eliminating water molecules, assigning hydrogen bonds, optimizing receptor atom charges, and performing energy minimization with the OPLS3 force field[98].

Glide standard precision (SP) ligand docking

Ligand docking was performed flexibly using the standard precision (SP) protocol within the Glide tool of Schrödinger-Maestro (version 11.5). To ensure accurate modeling, non-cis/trans amide bond configurations were penalized during the procedure. The Van der Waals forces for ligand atoms were adjusted with a scaling factor of 0.80, and a partial charge cutoff of 0.15 was applied. Docking results were analyzed using glide scores calculated from the energy-optimized ligand conformations. The conformation with the most favorable (lowest) glide score was identified as the optimal binding pose for each ligand[96].

ADMET analysis

The QikProp tool in Schrödinger's Maestro software (version 11.5) was used to estimate the ADMET (absorption, distribution, metabolism, and excretion) profiles of the studied molecules. These predictions were derived from their physicochemical and pharmacokinetic characteristics, such as molecular weight, the number of hydrogen bond donors and acceptors, total solvent-accessible surface area, blood–brain partitioning coefficient, octanol–water partition coefficient, and aqueous solubility[99].

Statistical Analysis

One-way analysis of variance (ANOVA) was used to statistically evaluate all collected data on the effectiveness of different extract concentrations. Using a significance threshold of 0.05, a post hoc analysis was performed to compare the means using the least significant difference test.

Data availability

The datasets used and/or analysed during the current study available from the corresponding author on reasonable request.

Received: 27 November 2024; Accepted: 7 March 2025
Published online: 28 March 2025

References

1. Akacha, B. B. et al. Recent advances in phytochemistry, pharmaceutical, biomedical, phytoremediation, and bio-preservative applications of *Lobularia maritima*. *S. Afr. J. Bot.* **165**, 202–216 (2024).
2. Pieracci, Y. et al. Antimicrobial activity and composition of five rosmarinus (*Now salvia* spp. and varieties) essential oils. *Antibiotics* **10**, 1090 (2021).
3. Macedo, L. M. et al. Rosemary (*Rosmarinus officinalis* L. syn Salvia rosmarinus Spenn.) and its topical applications: A review. *Plants* **9**, 651 (2020).
4. Alqethami, A. & Aldhebiani, A. Y. Medicinal plants used in Jeddah, Saudi Arabia: Phytochemical screening. *Saudi J. Biol. Sci.* **28**, 805–812 (2021).
5. Eftimová, J. & Nociarová, N. Influence of application forms of alginite on phytomass formation, bioactive contents and antioxidant activity of extracts from plants *Rosmarinus officinalis* L. *Agrobiodiversity for Improving Nutrition, Health and Life Quality* **6**, (2022).

6. Aamer, H. A. et al. Extraction, phytochemical characterization, and antifungal activity of Salvia rosmarinus extract. *Open Chem.* **21**, 20230124 (2023).
7. Elansary, H. O. et al. Saudi *Rosmarinus officinalis* and *Ocimum basilicum* L. polyphenols and biological activities. *Processes* **8**, 446 (2020).
8. Kabubii, Z. N., Mbaria, J. M., Mathiu, P. M., Wanjohi, J. M. & Nyaboga, E. N. Diet supplementation with Rosemary (*Rosmarinus officinalis* L) leaf powder exhibits an antidiabetic property in streptozotocin-induced diabetic male wistar rats. *Diabetology* **5**, 12–25 (2024).
9. Asiamah, I., Obiri, S. A., Tamekloe, W., Armah, F. A. & Borquaye, L. S. Applications of molecular docking in natural products-based drug discovery. *Sci. Afr.* **20**, e01593 (2023).
10. Pinzi, L. & Rastelli, G. Molecular docking: Shifting paradigms in drug discovery. *Int. J. Mol. Sci.* **20**, 4331 (2019).
11. Agu, P. et al. Molecular docking as a tool for the discovery of molecular targets of nutraceuticals in diseases management. *Sci. Rep.* **13**, 13398 (2023).
12. Patil, R. et al. Optimized hydrophobic interactions and hydrogen bonding at the target-ligand interface leads the pathways of drug-designing. *PLoS ONE* **5**, e12029 (2010).
13. Ilie, E. I. et al. Phytochemical characterization and antioxidant activity evaluation for some plant extracts in conjunction with pharmacological mechanism prediction: Insights into potential therapeutic applications in dyslipidemia and obesity. *Biomedicines* **12**, 1431 (2024).
14. Sucharitha, P., Reddy, K.R., Satyanarayana, S., Garg, T. Absorption, distribution, metabolism, excretion, and toxicity assessment of drugs using computational tools. In: *Computational approaches for novel therapeutic and diagnostic designing to mitigate SARS-CoV-2 infection*: Elsevier; 2022. pp. 335–355.
15. Durán-Iturbide, N. A., Díaz-Eufracio, B. I. & Medina-Franco, J. L. In silico ADME/Tox profiling of natural products: A focus on BIOFACQUIM. *ACS Omega* **5**, 16076–16084 (2020).
16. Kralj, S., Jukič, M. & Bren, U. Molecular filters in medicinal chemistry. *Encyclopedia* **3**, 501–511 (2023).
17. Mahapatra, S. R. et al. The potential of plant-derived secondary metabolites as novel drug candidates against Klebsiella pneumoniae: Molecular docking and simulation investigation. *S. Afr. J. Bot.* **149**, 789–797 (2022).
18. Ghafoori, H., Sariri, R. & Naghavi, M. STudy of effect of extraction conditions on the biochemical composition and antioxidant activity of *Artemisia absinthium* by HPLC and TLC. *J. Liq. Chromatogr. Related Technol.* **37**, 1558–1567 (2014).
19. Hendel, N. et al. Phytochemical analysis and antioxidant and antifungal activities of powders, methanol extracts, and essential oils from *Rosmarinus officinalis* L and *Thymus ciliatus* Desf. Benth.. *Int. J. Mol. Sci.* **25**, 7989 (2024).
20. Kamli, T. E. et al. Comparaison Quantitative Et Qualitative Des Huiles Essentielles De *Rosmarinus officinalis* Obtenues Par Différentes Méthodes. *Eur. Sci. J.* **13**, 1857–7881 (2017).
21. Cutillas, A.-B., Carrasco, A., Martinez-Gutierrez, R., Tomas, V. & Tudela, J. *Rosmarinus officinalis* L. essential oils from Spain Composition, antioxidant capacity, lipoxygenase and acetylcholinesterase inhibitory capacities, and antimicrobial activities. *Plant Biosyst. Int. J. Deal. Asp. Plant Biol.* **152**, 1282–1292 (2018).
22. Bozin, B., Mimica-Dukic, N., Samojlik, I. & Jovin, E. Antimicrobial and antioxidant properties of rosemary and sage (*Rosmarinus officinalis* L. and *Salvia officinalis* L., Lamiaceae) essential oils. *J. Agric. Food Chem.* **55**, 7879–7885 (2007).
23. Rašković, A. et al. Antioxidant activity of rosemary (*Rosmarinus officinalis* L.) essential oil and its hepatoprotective potential. *BMC Complement. Altern. Med.* **14**, 1–9 (2014).
24. Abada, M. B. et al. Variations in chemotypes patterns of Tunisian *Rosmarinus officinalis* essential oils and applications for controlling the date moth *Ectomyelois ceratoniae* (Pyralidae). *S. Afr. J. Bot.* **128**, 18–27 (2020).
25. Aprotosoaie, A. C., Luca, V. S., Trifan, A. & Miron, A. Antigenotoxic potential of some dietary non-phenolic phytochemicals. *Stud. Nat. Prod. Chem.* **60**, 223–297 (2019).
26. Mondal, A., Bose, S., Mazumder, K. & Khanra, R. (2021) Carvacrol (*Origanum vulgare*): Therapeutic properties and molecular mechanisms. *Bioactive Nat. Prod. Pharm. Appl.* 437–462.
27. Ijinu, T.P., Prabha, B., Pushpangadan, P. & George, V. Essential oil-derived monoterpenes in drug discovery and development. In: *Drug Discovery and Design Using Natural Products*: Springer; pp. 103–149 (2023).
28. Baginska, S., Golonko, A., Swislocka, R. & Lewandowski, W. Monoterpenes as medicinal agents: Exploring the pharmaceutical potential of p-cymene, p-cymenene, and γ-terpinene. *Acta Pol. Pharm.* **80**, 879–892 (2023).
29. Sulaiman, C. & Balachandran, I. Total phenolics and total flavonoids in selected Indian medicinal plants. *Indian J. Pharm. Sci.* **74**, 258 (2012).
30. Rafya, M., Zehhar, N., Hafidi, A. & Benkhalti, F. Review of *Rosmarinus officinalis* L. essential oil, hydrosol, and residues analysis: Composition, bioactivities, and valorization. *Ind. Crops Products* **221**, 119392 (2024).
31. Chaves, J. O. et al. Extraction of flavonoids from natural sources using modern techniques. *Fronti. Chem.* **8**, 507887 (2020).
32. Yeasmen, N. & Orsat, V. Green extraction and characterization of leaves phenolic compounds: A comprehensive review. *Crit. Rev. Food Sci. Nutr.* **63**, 5155–5193 (2023).
33. Al-jaafreh, A. M. Evaluation of antioxidant activities of rosemary (*Rosmarinus officinalis* L.) essential oil and different types of solvent extractions. *Biomed. Pharmacol. J.* **17**, 323–339 (2024).
34. Chaqroune, A. & Taleb, M. Effects of extraction technique and solvent on phytochemicals, antioxidant, and antimicrobial activities of cultivated and wild rosemary (*Rosmarinus officinalis* L.) from Taounate region. *Biointerface Res. Appl. Chem.* **12**, 8441–8452 (2022).
35. Mena P, Cirlini M, Tassotti M, Herrlinger KA, Dall'Asta C, Del Rio D.Phytochemical profiling of flavonoids, phenolic acids, terpenoids, and volatile fraction of a rosemary (*Rosmarinus officinalis* L) extract. *Molecules* **21**, 1576 (2016).
36. Andrés, C. M. C., Pérez de la Lastra, J. M., Juan, C. A., Plou, F. J. & Pérez-Lebeña, E. Polyphenols as antioxidant/pro-oxidant compounds and donors of reducing species: Relationship with human antioxidant metabolism. *Processes* **11**, 2771 (2023).
37. Ullah, F. et al. DPPH, ABTS free radical scavenging, antibacterial and phytochemical evaluation of crude methanolic extract and subsequent fractions of *Chenopodium botrys* aerial parts. *Pak. J. Pharm. Sci* **30**, 761–766 (2017).
38. Hendel, N., Larous, L. & Belbey, L. Antioxidant activity of rosemary (*Rosmarinus officinalis* L.) and its in vitro inhibitory effect on *Penicillium digitatum*. *Int. Food Res. J.* **23**, (2016).
39. Saini, A. et al. Assessment of antioxidant activity of rosemary (*Rosmarinus officinalis*) leaves extract. *J. Pharmacogn. Phytochem.* **9**, 14–17 (2020).
40. Shankar, A., Ali, A., Abdullah, H.M., Balaji, J., Kaur, J., Saeed, F., Wasiq, M., Imran, A. & Jibraeel, H., Raheem, M.S. Nutritional composition, phytochemical profile, therapeutic potentials, and food applications of rosemary: A comprehensive review. *J. Food Compos. Anal.* 106688 (2024).
41. Liu, X.-Y., Wang, W.-Z., Yao, S.-P., Li, X.-Y., Han, R.-M., Zhang, D., Zhao, Z., Wang Y, Zhang J-P. Antioxidation activity enhancement by intramolecular hydrogen bond and non-browning mechanism of active ingredients in rosemary: Carnosic acid and carnosol. *The J. Phys. Chem. B* (2024).
42. Gulcin, İ & Alwasel, S. H. DPPH radical scavenging assay. *Processes* **11**, 2248 (2023).
43. Ilyasov, I. R., Beloborodov, V. L., Selivanova, I. A. & Terekhov, R. P. ABTS/PP decolorization assay of antioxidant capacity reaction pathways. *Int. J. Mol. Sci.* **21**, 1131 (2020).
44. Koygun, G., Arslan, E., Zengin, G., Orlando, G. & Ferrante, C. Comparison of anticancer activity of *Dorycnium pentaphyllum* extract on MCF-7 and MCF-12A cell line: Correlation with invasion and adhesion. *Biomolecules* **11**, 671 (2021).

45. Coppola, L., Tait, S., Fabbrizi, E., Perugini, M. & La Rocca, C. Comparison of the toxicological effects of pesticides in non-tumorigenic MCF-12A and tumorigenic MCF-7 human breast cells. *Int. J. Environ. Res. Public Health* **19**, 4453 (2022).
46. Dai, J. et al. Roles of hormone replacement therapy and iron in proliferation of breast epithelial cells with different estrogen and progesterone receptor status. *The Breast* **17**, 172–179 (2008).
47. Romani, A. M. Cisplatin in cancer treatment. *Biochem. Pharmacol.* **206**, 115323 (2022).
48. Becer, E. et al. Composition and antibacterial, anti-inflammatory, antioxidant, and anticancer activities of *Rosmarinus officinalis* L. essential oil. *South Afr. J. Bot.* **160**, 437–445 (2023).
49. Wang, W., Li, N., Luo, M., Zu, Y. & Efferth, T. Antibacterial activity and anticancer activity of *Rosmarinus officinalis* L. essential oil compared to that of its main components. *Molecules* **17**, 2704–2713 (2012).
50. Cheung, S. & Tai, J. Anti-proliferative and antioxidant properties of rosemary *Rosmarinus officinalis*. *Oncol. Rep.* **17**, 1525–1531 (2007).
51. Tabatabaei, S.M., Kianinodeh, F., Nasiri, M., Tightiz, N., Asadipour, M. & Gohari, M. In vitro inhibition of MCF-7 human breast cancer cells by essential oils of *Rosmarinus officinalis*, *Thymus vulgaris* L., and Lavender x intermedia. *Archives of Breast Cancer* 81–89 (2018)
52. Đilas, S. et al. In vitro antioxidant and antiproliferative activity of three rosemary (*Rosmarinus officinalis* L.) extract formulations. *Int. J. Food Sci. Technol.* **47**, 2052–2062 (2012).
53. Mothana, R. A., Kriegisch, S., Harms, M., Wende, K. & Lindequist, U. Assessment of selected Yemeni medicinal plants for their in vitro antimicrobial, anticancer, and antioxidant activities. *Pharm. Biol.* **49**, 200–210 (2011).
54. Chaudhry G-e-S, Md., Akim, A., Sung, Y. Y. & Sifzizul, T. M. T. Cancer and apoptosis: The apoptotic activity of plant and marine natural products and their potential as targeted cancer therapeutics. *Front. Pharmacol.* **13**, 842376 (2022).
55. Amini Navaie, B. et al. Antioxidant and cytotoxic effect of aqueous and hydroalcoholic extracts of the *Achillea millefolium* L. on MCF-7 breast cancer cell line. *Int. Biol. Biomed. J.* **1**, 119–125 (2015).
56. Awad, B. M. et al. Cytotoxic activity evaluation and molecular docking study of phenolic derivatives from *Achillea fragrantissima* (Forssk) growing in Egypt. *Med. Chem. Res.* **26**, 2065–2073 (2017).
57. Sharma, M. et al. Essential oils as anticancer agents: Potential role in malignancies, drug delivery mechanisms, and immune system enhancement. *Biomed. Pharmacotherapy* **146**, 112514 (2022).
58. Gîrd, C. E., Costea, T. & Mitran, V. Evaluation of cytotoxic activity and anticancer potential of indigenous Rosemary (*Rosmarinus officinalis* L.) and Oregano (*Origanum vulgare* L.) dry extracts on MG-63 bone osteosarcoma human cell line. *Rom. J. Morphol. Embryol.* **62**, 525 (2021).
59. Jang, Y.-G., Hwang, K.-A. & Choi, K.-C. Rosmarinic acid, a component of rosemary tea, induced the cell cycle arrest and apoptosis through modulation of HDAC2 expression in prostate cancer cell lines. *Nutrients* **10**, 1784 (2018).
60. Jiang, M., Qi, L., Li, L. & Li, Y. The caspase-3/GSDME signal pathway as a switch between apoptosis and pyroptosis in cancer. *Cell Death Discov.* **6**, 112 (2020).
61. Pfeffer, C. M. & Singh, A. T. Apoptosis: A target for anticancer therapy. *Int. J. Mol. Sci.* **19**, 448 (2018).
62. Damić, A. M. & Matejić, J. S. Plant products in the prevention of diabetes mellitus. *Mini Rev. Med. Chem.* **22**, 1395–1419 (2022).
63. Sharma, A. D., Inderjeet, K., Jaspreet, K. & Chauhan, A. Chemical profiling and in-vitro anti-oxidant, anti-diabetic, anti-inflammatory, anti-bacterial and anti-fungal activities of essential oil from *Rosmarinus officinalis* L.. *Notulae Sci. Biol.* **16**, 11756–11756 (2024).
64. McCue. P.P., & Shetty, K. Inhibitory effects of rosmarinic acid extracts on porcine pancreatic amylase in vitro. *Asia Pac. J. Clin. Nutr.* **13** (2004).
65. Bakırel, T., Bakırel, U., Keleş, O. Ü., Ülgen, S. G. & Yardibi, H. In vivo assessment of antidiabetic and antioxidant activities of rosemary (*Rosmarinus officinalis*) in alloxan-diabetic rabbits. *J. Ethnopharmacol.* **116**, 64–73 (2008).
66. Vaou, N., Stavropoulou, E., Voidarou, C., Tsigalou, C. & Bezirtzoglou, E. Towards advances in medicinal plant antimicrobial activity: A review study on challenges and future perspectives. *Microorganisms* **9**, 2041 (2021).
67. Celiktas, O. Y. et al. Antimicrobial activities of methanol extracts and essential oils of *Rosmarinus officinalis*, depending on location and seasonal variations. *Food Chem.* **100**, 553–559 (2007).
68. Soliman, M. M., Elsaba, Y. M., Soliman, M. & Ahmed, E. Z. Composition and antimicrobial activity of *Rosmarinus officinalis* L. and *Artemisia monosperma* L. leaf essential oils and methanolic extracts from plants grown in normal and saline habitats in Egypt. *Sci. Rep.* **14**, 7342 (2024).
69. Jafari-Sales, A. & Hossein-Nezhad, P. Antimicrobial effects of *Rosmarinus officinalis* methanolic extract on *Staphylococcus aureus*, *Bacillus cereus*, *Escherichia coli* and *Pseudomonas aeruginosa* in laboratory conditions. *J. Med. Chem. Sci.* **3**, 103–108 (2020).
70. Hou, T. et al. Essential oils and its antibacterial, antifungal and anti-oxidant activity applications: A review. *Food Biosci.* **47**, 101716 (2022).
71. Steinbuch, K. B. & Fridman, M. Mechanisms of resistance to membrane-disrupting antibiotics in gram-positive and gram-negative bacteria. *MedChemComm* **7**, 86–102 (2016).
72. Greenfield, D. A. et al. Virtual screening for ligand discovery at the σ1 receptor. *ACS Med. Chem. Lett.* **11**, 1555–1561 (2020).
73. Butterworth, P. J., Warren, F. J. & Ellis, P. R. Human α-amylase and starch digestion: An interesting marriage. *Starch-Stärke* **63**, 395–405 (2011).
74. Kumar, A. et al. Apoptosis-mediated anti-proliferative activity of *Calligonum comosum* against human breast cancer cells, and molecular docking of its major polyphenolics to Caspase-3. *Front. Cell Dev. Biol.* **10**, 972111 (2022).
75. Collin, F., Karkare, S. & Maxwell, A. Exploiting bacterial DNA gyrase as a drug target: Current state and perspectives. *Appl. Microbiol. Biotechnol.* **92**, 479–497 (2011).
76. Sun, L., Wang, Y. & Miao, M. Inhibition of α-amylase by polyphenolic compounds: Substrate digestion, binding interactions and nutritional intervention. *Trends Food Sci. Technol.* **104**, 190–207 (2020).
77. Gallivan, J. P. & Dougherty, D. A. Cation-π interactions in structural biology. *Proc. Natl. Acad. Sci.* **96**, 9459–9464 (1999).
78. Headen, T. F. et al. Structure of π– π interactions in aromatic liquids. *J. Am. Chem. Soc.* **132**, 5735–5742 (2010).
79. Kurczab, R., Śliwa, P., Rataj, K., Kafel, R. & Bojarski, A. J. Salt bridge in ligand–protein complexes—systematic theoretical and statistical investigations. *J. Chem. Inf. Model.* **58**, 2224–2238 (2018).
80. Lipinski, C. A., Lombardo, F., Dominy, B. W. & Feeney, P. J. Experimental and computational approaches to estimate solubility and permeability in drug discovery and development settings. *Adv. Drug Deliv. Rev.* **64**, 4–17 (2012).
81. Artursson, P., Palm, K. & Luthman, K. Caco-2 monolayers in experimental and theoretical predictions of drug transport. *Adv. Drug Deliv. Rev.* **46**, 27–43 (2001).
82. Wolfe, K. L. & Liu, R. H. Apple peels as a value-added food ingredient. *J. Agric. Food Chemistry* **51**, 1676–1683 (2003).
83. Ordonez, A., Gomez, J. & Vattuone, M. Antioxidant activities of *Sechium edule* (Jacq.) Swartz extracts. *Food Chem.* **97**, 452–458 (2006).
84. Tian, M. et al. Phytochemical analysis, antioxidant, antibacterial, cytotoxic, and enzyme inhibitory activities of *Hedychium flavum* rhizome. *Front. Pharmacol.* **11**, 572659 (2020).
85. Reviana, R. et al. Analysis of antioxidant activity on cocktail honey products as female pre-conception supplements. *Gaceta Sanit.* **35**, S202–S205 (2021).
86. Yu, X., Zhao, M., Liu, F., Zeng, S. & Hu, J. Antioxidants in volatile Maillard reaction products: Identification and interaction. *LWT-Food Sci. Technol.* **53**, 22–28 (2013).

87. Ghasemi, M., Turnbull, T., Sebastian, S. & Kempson, I. The MTT assay: Utility, limitations, pitfalls, and interpretation in bulk and single-cell analysis. *Int. J. Mol. Sci.* **22**, 12827 (2021).
88. Al-Dhabi, N.A. & Valan Arasu, M. Quantification of phytochemicals from commercial Spirulina products and their antioxidant activities. *Evid.-Based Complement. Altern. Med.* **2016**, (2016).
89. Aziz, I. M. et al. Chemical composition, antioxidant, anticancer, and antibacterial activities of roots and seeds of *Ammi visnaga L.* methanol extract. *Pharmaceuticals* **17**, 121 (2024).
90. Wickramaratne, M. N., Punchihewa, J. & Wickramaratne, D. In-vitro alpha amylase inhibitory activity of the leaf extracts of *Adenanthera pavonina*. *BMC Complement. Altern. Med.* **16**, 1–5 (2016).
91. Kim, Y.-M., Wang, M.-H. & Rhee, H.-I. A novel α-glucosidase inhibitor from pine bark. *Carbohydr. Res.* **339**, 715–717 (2004).
92. Salem, N. et al. Variation in chemical composition of *Eucalyptus globulus* essential oil under phenological stages and evidence synergism with antimicrobial standards. *Indust. Crops Prod.* **124**, 115–125 (2018).
93. Basri, D.F. & Sandra, V. Synergistic interaction of methanol extract from *Canarium odontophyllum* Miq. Leaf in combination with oxacillin against methicillin-resistant *Staphylococcus aureus* (MRSA) ATCC 33591. *Int. J. Microbiol.* **2016** (2016)
94. Aljeldah, M.M., Yassin, M.T., Mostafa, A.A.-F. & Aboul-Soud, M.A. Synergistic antibacterial potential of greenly synthesized silver nanoparticles with fosfomycin against some nosocomial bacterial pathogens. *Infect. Drug Res.* 125–142 (2022).
95. Mssillou, I., Agour, A., Lefrioui, Y. & Chebaibi, M. LC-TOFMS analysis, in vitro and in silico antioxidant activity on NADPH oxidase, and toxicity assessment of an extract mixture based on *Marrubium vulgare* L. and *Dittrichia viscosa* L. *J. Biol. Biomed. Res.* **1**, 31–45 (2024).
96. Bouslamti, M. et al. Phenolic profile, inhibition of α-amylase and α-glucosidase enzymes, and antioxidant properties of *Solanum elaeagnifolium* Cav. (Solanaceae): In vitro and in silico investigations. *Processes* **11**, 1384 (2023).
97. Alsaleh, A. N. et al. In vitro evaluation, chemical profiling, and in silico ADMET prediction of the pharmacological activities of *Artemisia absinthium* root extract. *Pharmaceuticals* **17**, 1646 (2024).
98. Tourabi, M. et al. Antioxidant, antimicrobial, and insecticidal properties of chemically characterized essential oils extracted from *Mentha longifolia* in vitro and in silico analysis. *Plants* **12**, 3783 (2023).
99. Chebaibi, M. et al. Antiviral activities of compounds derived from medicinal plants against SARS-CoV-2 based on molecular docking of proteases. *J. Biol. Biomed. Res.* **1**, 10–30 (2024).

Acknowledgements

The authors thank the Researchers Supporting Project number (RSPD2025R933), King Saud University, Riyadh, Saudi Arabia.

Author contributions

K.A.A and I.M.A. wrote the main manuscript text. I.M.A, M.A.F., T.A., and A.A.A. Mainly responsible for providing data. I.M.A., and A.M.A. are responsible for charting R.M.A is responsible for writing—review, editing, and language of the manuscript revision. All authors reviewed the manuscript.

Competing interests

The authors declare no competing interests.

Ethical conduct of research

The conducted research is not related to either human or animal use. However, the collection of plant materials was conducted following the guidelines of the International Union for Conservation of Nature (IUCN) policies research involving species at risk of extinction and the Convention on the Trade in Endangered Species of Wild Fauna and Flora. The cell lines were provided by the Virology Research Laboratory (VRG) group, College of Science, King Saud University, Saudi Arabia. All cell lines were maintained at 37 ℃ in and were mycoplasma-free (LookOut® Mycoplasma qPCR Detection Kitm, MERK).

Additional information

Correspondence and requests for materials should be addressed to I.M.A.

Reprints and permissions information is available at www.nature.com/reprints.

Publisher's note Springer Nature remains neutral with regard to jurisdictional claims in published maps and institutional affiliations.